

Quantifying prevalence and risk factors of HIV multiple infection in Uganda from cross-sectional population-based deep-sequence data

Michael A. Martin^{1,†}, Andrea Brizzi², Xiaoyue Xi^{2,3}, Ronald Moses Galiwango⁴, Sikhulile Moyo^{5,6}, Deogratius Ssemwanga^{7,8}, Alexandra Blenkinsop², Andrew D. Redd^{9,10,11}, Lucie Abeler-Dörner¹², Christophe Fraser¹², Steven J. Reynolds^{4,9,10}, Thomas C. Quinn^{4,9,10}, Joseph Kagaayi^{4,13}, David Bonsall¹⁴, David Serwadda⁴, Gertrude Nakigozi⁴, Godfrey Kigozi⁴, M. Kate Grabowski^{1,4,15,†}, Oliver Ratmann^{2,†}, with the PANGEA-HIV Consortium and the Rakai Health Sciences Program

1 Department of Pathology, Johns Hopkins School of Medicine, Baltimore, MD, USA

2 Department of Mathematics, Imperial College London, London, United Kingdom

3 Medical Research Council Biostatistics Unit, University of Cambridge, Cambridge, UK

4 Rakai Health Sciences Program, Kalisizo, Uganda

5 Botswana Harvard AIDS Institute Partnership, Botswana Harvard HIV Reference Laboratory, Gaborone, Botswana

6 Harvard T.H. Chan School of Public Health, Boston, MA, USA

7 Medical Research Council/Uganda Virus Research Institute and London School of Hygiene and Tropical Medicine Uganda Research Unit, Entebbe, Uganda

8 Uganda Virus Research Institute, Entebbe, Uganda

9 Department of Medicine, Johns Hopkins School of Medicine, Baltimore, MD, USA

10 Division of Intramural Research, National Institute of Allergy and Infectious Diseases, National Institutes of Health, Bethesda, MD, USA

11 Institute of Infectious Disease and Molecular Medicine, University of Cape Town, Cape Town, South Africa

12 Pandemic Sciences Institute, Nuffield Department of Medicine, University of Oxford, Oxford, UK

13 Makerere University School of Public Health, Kampala, Uganda

14 Wellcome Centre for Human Genetics, Nuffield Department of Medicine, University of Oxford, Oxford, UK

15 Department of Epidemiology, Johns Hopkins Bloomberg School of Public Health, Baltimore, MD, USA

† Corresponding authors mmart108@jhmi.edu, mgrabow2@jhu.edu, oliver.ratmann@imperial.ac.uk

Abstract

People living with HIV can be simultaneously infected with genetically distinct variants. This can occur either at the time of initial infection (“coinfection”) or at a later time-point (“superinfection”). Multiple infection provides the necessary conditions for the generation of novel recombinant forms of HIV and may worsen clinical outcomes and increase the rate of transmission to HIV seronegative sexual partners. To date, studies of HIV multiple infection have relied on insensitive bulk-sequencing, labor intensive single genome amplification protocols, or deep-sequencing of short genome regions. Here, we present the Bayesian deep-phylo multiple infection model (*deep-phyloMI*), designed to identify multiple infections from whole-genome or near whole-genome pathogen deep-sequence data. This model simultaneously estimates individual- and population-level probabilities of harboring a multiple infection while accounting for partial sequencing success and false-negative and false-positive detection rates. We fit this model to HIV deep-sequence data generated from 2,029 people living with viremic HIV who participated in the population-based Rakai Community Cohort Study and estimate that 5.79% (95% HPD 4.56% - 7.07%) of sequenced participants harbor a multiple infection. Further, we show that participants living in high-HIV prevalence communities along Lake Victoria are 2.04-fold (95% HPD 1.15 - 3.22) more likely to harbor a multiple infection compared to individuals in lower prevalence neighboring communities. This work introduces a surveillance framework for identifying people with multiple HIV infections and quantifying population-level prevalence and risk factors of multiple infection for clinical and epidemiological investigations.

Author summary

HIV exists as a population of genetically distinct viral variants among people living with HIV. People living with HIV can be infected with genetically distinct variants. Identification of these mixed infections requires generating viral genomic data from people living with HIV. In the past, the approaches used to identify multiple infections from viral genomic data have had poor sensitivity or required labor intensive protocols that are prohibitive in application to large data sets. Prior work has also only utilized data generated from only small portions of the viral genome and the statistical procedures used to generate population-level estimates from sequencing data generated from individual infections has not accounted for incomplete sampling of the within-host viral population or sources of sequencing error, which may confound multiple infection estimates. Here, we develop a statistical model that addresses these limitations and allows for the identification of multiple infections and the estimation of population-level risk of multiple infection from deep-sequence data. We fit this model to population-based HIV genomic data from people living with HIV in southern Uganda and estimate that approximately 6% of viremic participants harbor a multiple infection at a given point in time. We show that the prevalence of multiple infections is higher in key populations with high HIV prevalence. These findings inform our understanding of the sexual risk networks that give rise to multiple infections and aid in efforts to model HIV epidemiological dynamics and evolution during a period of incidence declines and shifting transmission dynamics across Eastern and Southern Africa.

1 Introduction

Simultaneous infection with multiple lineages of human immunodeficiency virus (HIV) can occur at the time of initial infection [1] or through secondary infection [2]. Following acquisition, infecting lineages are shaped by within-individual evolutionary processes and can either stably coexist or undergo competitive exclusion [3, 4]. The acquisition of multiple simultaneous infections by PLHIV has important implications for the evolution, pathogenesis, and spread of HIV. Specifically, it provides the necessary conditions for the generation of novel recombinant viruses [5–7], which fuels diversification of the circulating viral population [8, 9], complicating vaccine development efforts through the generation of novel epitopes [10, 11] and potentially leads to the evolution of more transmissible viral genotypes [12]. Further, multiple infections may themselves lead to faster disease progression [13–15] and higher viral load [14–16], thereby potentially also increasing the risk of onward transmission [17, 18]. While the availability of viral genome sequence data has allowed for the identification of HIV multiple infections across a range of epidemiological contexts [19], prevalence estimates have generally been based on relatively small samples sizes with only partial genome data. Here, we identify HIV multiple infections using within-host deep-sequence phylogenetic trees inferred across the genome from a population-based surveillance cohort.

To date, viral sequence-based methods to identify HIV multiple infections generally rely on one of three approaches. First, bulk sequencing (e.g. Sanger sequencing or consensus sequence estimation from deep-sequence data) can reveal instances where the majority viral variant changes between baseline and follow-up visits under longitudinal sampling or cases where the within-person viral population at a specific visit harbors abnormal levels of diversity [14, 20–22]. This approach, however, has poor sensitivity, particularly when the proportion of the viral population belonging to one of the variants is small [23]. Alternatively, single genome amplification (SGA) relies on serial dilutions to isolate a single molecule of transcribed viral cDNA prior to amplification and sequencing. This approach is more sensitive in detecting minor variants than bulk sequencing [24–28], but is labor intensive and difficult to apply at scale. Amplicon deep-sequencing of discrete regions of the HIV genome is able to achieve high sensitivity while being highly scalable to large sets of samples [3, 24, 29–31].

Despite advancements in viral sequence-based identification of HIV multiple infections, existing approaches share shortcomings that hinder the interpretation of the results they generate. Critically, all of these methods rely on sequence data generated from only a subset of the genome, due in part to historical challenges in generating whole-genome HIV sequence data. For example, general population-based studies in Rakai, Uganda have previously utilized sequence data from 390 base pairs (bp) and 324 bp of the p24 (*gag*) and gp41 (*env*) regions, representing only 7.3% of the HIV genome. This inherently limits sensitivity to identify multiple infection with viral variants that are highly related within these short regions. Analysis of *gag* sequence data sampled from high-risk Kenyan women revealed cases of superinfection that were unidentified

when querying only the *env* region [32]. Further, limited consideration has been given to the fact that factors that affect sequencing success of biological samples [33] may also affect the detection probability of multiple viral variants and may therefore confound prevalence estimates and assessment of multiple infection risk factors. Finally, existing methods use binary categorization of samples as either multiply or singly infected. They do not quantify uncertainty in individual-level assignments and do not account for this uncertainty when estimating population-level prevalence. With the advent of approaches that can generate near whole-genome HIV deep-sequence data [33,34], there is a need for statistical approaches that can integrate data from across the genome to robustly identify multiple infections while accounting for the various sources of bias that can obscure the underlying biological signal.

Here, we provide estimates of the prevalence of HIV multiple infections and risk factors for harboring a multiple infection based on HIV deep-sequence data sampled from 2,029 people living with viremic HIV aged 15-49 who participated in the longitudinal, population-based Rakai Community Cohort Study [35,36] between October 2010 and May 2019. Rakai District is located in south-central Uganda, East Africa, bordering Lake Victoria, and is one of the areas with highest HIV-prevalence globally [28]. To support these inferences, we developed a novel Bayesian statistical model to identify multiple infections using within-host phylogenetic trees inferred from deep-sequence data generated from across the HIV genome, which we call the deep-phylo multiple infection model (*deep-phyloMI*). *Phyloscanner* [37] was used to infer within-host phylogenetic trees across the HIV genome, remove contaminant sequences, and identify regions of the genome with evidence of multiple infecting variants. Our model simultaneously estimates individual- and population-level risks of harboring a multiple infection from processed *phyloscanner* output after accounting for incomplete sequencing of the viral population within a sample and false-negative and false-positive rates of multiple variant identification. We validated model performance on simulated data and used it to identify RCCS participants harboring multiple infections, estimated prevalence of multiple infection among viremic RCCS participants and identified epidemiological risk factors of harboring multiple infections across sub-populations with heterogeneous risk behaviour at a time when incidence is declining rapidly and transmission dynamics are shifting [35,38].

2 Materials and methods

2.1 Study design and participants

The RCCS conducts population-based surveys every 18-24 months in agrarian, semi-urban trading, and Lake Victoria fishing communities in southern Uganda. Data in this study were collected over six RCCS survey rounds conducted between 2010 and 2020. As survey rounds occurred over more than a year, we herein refer to them by the median interview date. Communities that participated in the RCCS were categorized based on their geographic setting and primary economic activity (inland communities: agrarian / trading, Lake Victoria communities: fishing). These communities differ considerably in their HIV burden (HIV prevalence of ~14% [agrarian], ~17% [trading], and ~42% [fishing]) [36]. At each survey round, households were censused and all residents aged 15-49 who were able to provide consent (assent for those under 18) were invited to participate in a survey. Survey participants were eligible to participate exactly once in each survey round (“participant-visits”). As part of the survey, participants completed a detailed structured sociodemographic, behavioral, and health questionnaire. Specifically, participants were asked to self-report their sex, age, residency status (e.g. recent migration into a community), circumcision status (among males), occupation, occupation of sex partners in the year prior to the survey, and number of lifetime sex partners. As HIV is more prevalent among female sex and bar/restaurant workers [39,40], we generated a composite variable indicating reported sex or bar/restaurant work among women and sex with a sex or bar/restaurant worker among men to determine if these individuals were at higher risk of being multiply infected.

To account for the fact that the number of lifetime sex partners increases over the lifespan, we calculated the mean number of lifetime sex partners within population strata (s) defined by HIV serostatus, sex, age category in five year bins, and community type (inland / fishing) (\bar{P}_s) to allow for standardization of the observed responses. Responses of no lifetime sex partners were treated as missing data as HIV transmission in this setting is predominantly heterosexual [41] and we therefore expected these individuals to have had at least one sexual encounter in order to acquire HIV, although we cannot rule-out perinatal transmission with available data. When calculating \bar{P}_s missing data was imputed to the mean value of a lognormal distribution fit to all numeric responses of ≥ 1 lifetime sex partner within strata defined by HIV serostatus,

sex, age category, and community type. Additionally, some RCCS participants provided categorical responses (“1-2” and “3+” lifetime sex partners). To calculate P_s , we first imputed these values to a numeric response. Responses of “1-2” were imputed to the mean response among PLHIV reporting either one or two lifetime sex partners within strata. Similarly, responses of “3+” were imputed to the mean value of a lognormal distribution fit to all numeric responses of ≥ 3 lifetime partners within strata as above.

In addition to completing the survey questionnaire, participants provided venous blood samples for HIV testing, viral load quantification, and viral deep sequencing. HIV serostatus was evaluated using a validated rapid test algorithm [42]. HIV viral load quantification was conducted using the Abbott real-time m2000 assay (Abbott Laboratories). All participants provided written informed consent for the study. The RCCS is administered by the Rakai Health Sciences Program (RHSP) and has received ethical approval from the Uganda Virus Research Institute’s Research and Ethics Committee (HS540), the Uganda National Council for Science and Technology (GC/127/08/12/137), and the Johns Hopkins School of Medicine (IRB00217467).

2.2 HIV deep sequencing and bioinformatic processing

HIV deep-sequence data from RCCS participants was generated through the Phylogenetics and Networks for Generalized HIV Epidemics in Africa consortium (PANGEA-HIV) [43, 44]. Phylogenetic inference was performed using all available deep-sequence data for each participant. To avoid biasing our inferences, for individuals that participated in multiple survey rounds we used only the data from the sample with the highest genome coverage or the highest viral load in the case of ties in our analyses. As sequencing quality decreases at lower viral loads [33], we included only samples from viremic ($\geq 1,000$ copies/mL) PLHIV.

Deep-sequencing was performed with two protocols (S1 Table), as previously described [38]. Briefly, for sequence data generated through the amplicon protocol, viral RNA was extracted from plasma samples on the QIA Symphony SP workstation with the QIA Symphony DSP Virus/Pathogen Kit. cDNA was generated through one-step reverse transcription PCR protocol using universal HIV-1 primers designed to generate four overlapping amplicons across the HIV-1 genome [34]. Deep-sequencing was conducted at the Wellcome Trust Sanger Institute core facility using the Illumina MiSeq and HiSeq platforms. To generate sequence data using the bait-capture protocol viral RNA was similarly extracted using the QIA Symphony DSP Virus/Pathogen Kit followed by library preparation according to the veSEQ-HIV protocol [33]. Library preparation was performed using the SMARTer Stranded Total RNA-Seq v2-PicoInputMammalian (Clontech, TakaRaBio) kit and double-stranded dual-indexed cDNA generated using in-house indexed primers. Libraries were pooled and cleaned with Agencourt AMPure XMP. Pooled libraries were hybridized to HIV-specific biotinylated 120-mer oligonucleotides (xGen Lockdown Probes, Integrated DNA Technologies) and isolated with streptavidin-conjugated beads. Captured libraries were PCR amplified prior to generation of 350-600 base pair (bp) paired-ends reads with the Illumina NovaSeq 6000 at the Oxford Genomic Centre.

Kraken v.0.10.5-beta [45] with a custom database of human, bacterial, archaeal, viral, and fungal genomes was used to isolate reads of viral and unknown origin which were trimmed of adaptors and low-quality bases using trimmomatic [46] v.0.36/0.39. Trimmed reads were *de novo* assembled into contigs using SPAdes [47] and metaSPAdes [48] v.3.10. Shiver v.1.5.7 [49] was used to align reads to a reference sequence constructed for each sample using these contigs.

2.3 Inference of within-host deep-sequence phylogenetic trees

To improve the computational efficiency of our within-host deep-sequence phylogenetic analysis we first clustered participants with HIV into putative transmission networks as previously described (S1 File) [38, 50], and then grouped putative networks into batches for deep-sequence phylogenetic analyses.

Deep-sequence data belonging to participants in each batch were further processed with *phyloscanner* [37] v.1.8.1 to infer within-host phylogenetic trees in 287 sliding windows of length 250 bp with a step size of 25 across the HIV genome as in [38]. Windows around the envelope (*env*) glycoprotein variable loop regions were excluded as genetic diversity in this portion of the genome [51] led to poor sequence alignment and unreliable within-host phylogenetic trees. In addition to deep-sequence data from RCCS participants, we included as phylogenetic background 113 consensus sequences from representative subtypes and circulating forms and 200 near full-length consensus sequences from Kenya, Uganda, and Tanzania (Los Alamos National Laboratory HIV Sequence Database, <http://www.hiv.lanl.gov>, S2 File). Within *phyloscanner*, MAFFT

v.7.475 [52] with iterative refinement and iterative re-alignment using consistency scores was used to align sequencing reads and IQ-TREE v.2.0.3 with the GTR+F+R(Free-Rate)6 substitution model was used for phylogenetic inference [53,54]. Phylogenetic branch lengths within *phyloscanner* were adjusted to account for varying substitution rates across the HIV genome as described in [55] (S3 File). Adjusted distances can be interpreted as average distances expected in the *pol* gene. The genomic coordinates of input sequence data were standardized to the coordinates of the HIV-1 HXB2 reference genome (GenBank: K03455.1).

For each participant, *phyloscanner* was used to estimate the number of genetically distinct phylogenetic lineages (subgraphs) in each genome window using a modified parsimony algorithm. In each window, for each participant, the given phylogenetic tree was pruned to include only tips from the given participant and the specified outgroup (here, the subtype H consensus sequence). Ancestral nodes in the pruned tree were assigned to one of two states: either that of the participant or an unsampled “unassigned” state (to which the outgroup and root of the phylogeny was assigned), representing the lineages that are evolutionarily ancestral to the lineages that initiated a given host’s infection. To accurately assign nodes without relying on patterns of phylogenetic clustering with reference sequences, we employed a modified Sankoff minimum parsimony algorithm for ancestral state reconstruction as described in [37,56]. This algorithm assigns a cost ($c(n, h)$) to a state change along a lineage ending at ancestral node n that is proportional to the sum of the branch lengths descendant from that node that give rise to tips from host h ($l(n, h)$). As tips from all other subjects with the exception of the outgroup were pruned from the tree prior to this procedure, this is equivalent to the sum of the total branch length of the subtree with node n as its root. Specifically, this cost was calculated as:

$$c(n, h) = 1 + k \times l(n, h), \quad (1)$$

where k is a tuneable constant that controls the penalty associated with fewer host h subgraphs. Traditional parsimony is recovered when $k = 0$. As $k \rightarrow \infty$, each tip belonging to host h will be assigned to a unique subgraph. Here, we parameterized k with the goal of distinguishing evolutionary divergence that occurred within a host over the course of infection from that which occurred prior to a given host becoming infected. We conservatively used a k value of 15 such that $\frac{1}{k} = 0.067$, which is greater than the 99th percentile of the pairwise genetic distances between epidemiologically confirmed HIV transmission pairs [55] and comparable to within-subtype HIV genetic diversity within Rakai [9].

Quality filtering of inferred within-participant phylogenetic trees was performed with *phyloscanner*. Specifically, within each window, subgraphs with less than three reads or less than 1% of reads from a particular participant were marked as putative contaminants and removed from the analysis. To mask regions with insufficient data for reliable phylogenetic inference any window with less than 30 reads from a given participant after aforementioned filter was also removed from the analysis. After filtering we identified the subgraphs with data from the deep-sequenced reads from each sequenced sample for a given participant.

2.4 Bayesian model to identify multiple infections

We developed a Bayesian statistical model to identify samples harboring multiple infections and estimate the prevalence of multiple infections in a set of deep-sequencing reads that were processed with *phyloscanner*. We refer to this model as the the deep-phylo multiple infection model (*deep-phyloMI*). We first summarized the *phyloscanner* output for each sample and each genomic window in terms of two binary variables, $N_{i=1\dots n,w}^{\text{obs}}$ (presence/absence of sequencing reads from sample i in window w following *phyloscanner* contamination filtering) and $M_{i=1\dots n,w}^{\text{obs}}$ (presence/absence of multiple subgraphs for sample i in window w) where n is the number of sequenced samples. To simplify notation below, when $N_{i,w}^{\text{obs}} = 0$ we set $M_{i,w}^{\text{obs}} = 0$. We further summarized the data for sample i into two quantities, $N_i^{\text{obs}} = \sum_{w=1}^{n^{\text{max}}} N_{i,w}^{\text{obs}}$ and $M_i^{\text{obs}} = \sum_{w=1}^{n^{\text{max}}} M_{i,w}^{\text{obs}}$ where n^{max} is the number of genome windows. We include only data corresponding to the sample with the highest genome coverage (as measured by N_i^{obs}) and highest viral load in the case of ties for each participant. Samples with N_i^{obs} were excluded. Only participants with available deep-sequence data with a paired viral load measurement $\geq 1,000$ copies/mL were included in our inference method.

2.4.1 Base model accounting for partial sequencing success of infecting variants

We first developed a base model that accounts for partial sequencing success across the HIV genome in giving rise to the observed $N_{i=1\dots n,w}^{\text{obs}}$ and $M_{i=1\dots n,w}^{\text{obs}}$. Working from first principles, we derived a likelihood model

for observing the pair of counts $(N_i^{\text{obs}}, M_i^{\text{obs}})$ for the unobserved groups of individuals with multiple infection ($M_i = 1$) and with single infection ($M_i = 0$). Among multiply infected individuals ($M_i = 1$), we assumed that the probability of sequencing each of the infecting variants in window w was given by θ_i for each sample i . The probability of sequencing at least one variant in each window is therefore $1 - (1 - \theta_i)^2$ and the probability of sequencing both variants given at least one was sequenced is therefore $\frac{\theta_i}{2 - \theta_i}$. Assuming sequencing success was independently and identically distributed for each individual, we obtained

$$(N_i^{\text{obs}} | \theta_i, M_i = 1) \sim \text{Binomial}^{1+}(n^{\text{max}}, 1 - (1 - \theta_i)^2) \quad (2a)$$

$$(M_i^{\text{obs}} | N_i^{\text{obs}}, \theta_i, M_i = 1) \sim \text{Binomial}\left(N_i^{\text{obs}}, \frac{\theta_i}{2 - \theta_i}\right), \quad (2b)$$

where Binomial^{1+} represents the 0-truncated Binomial distribution as we only consider data from individuals with *phyloscanner* output in at least one genomic window and n^{max} is the total number of genomic windows. This model implicitly accounts for the presence of windows in which only a single variant was present in the *phyloscanner* output due to incomplete sequencing success. For individuals infected with only a single variant ($M_i = 0$), we obtained analogously

$$(N_i^{\text{obs}} | \theta_i, M_i = 0) \sim \text{Binomial}^{1+}(n^{\text{max}}, \theta_i) \quad (3a)$$

$$(M_i^{\text{obs}} | N_i^{\text{obs}}, \theta_i, M_i = 0) \sim \text{Binomial}(N_i^{\text{obs}}, 0). \quad (3b)$$

Taken together, the joint likelihood of observing the count pair $(M_i^{\text{obs}}, N_i^{\text{obs}})$ conditional on latent multiple infection status M_i is given by 182
183

$$P(N_i^{\text{obs}}, M_i^{\text{obs}} | \theta_i, M_i) = P(N_i^{\text{obs}} | \theta_i, M_i) P(M_i^{\text{obs}} | N_i^{\text{obs}}, \theta_i, M_i). \quad (4)$$

Thus, aggregating over the two unknown possible multiple infection states $M_i \in \{0, 1\}$ for each individual in a finite mixture model framework, we have 184
185

$$P(N_i^{\text{obs}}, M_i^{\text{obs}} | \theta_i) = \sum_{m=0,1} P(N_i^{\text{obs}} | \theta_i, M_i = m) P(M_i^{\text{obs}} | N_i^{\text{obs}}, \theta_i, M_i = m) P(M_i = m). \quad (5)$$

One of our primary inferential targets was the individual-level probability of harboring multiple infection not conditional on observed N_i^{obs} and M_i^{obs} , which we denoted with $\delta_i = P(M_i = 1)$. Making this target explicit in the joint likelihood, we have

$$P(N_i^{\text{obs}}, M_i^{\text{obs}} | \theta_i, \delta_i) = \quad (6a)$$

$$\delta_i P(N_i^{\text{obs}} | \theta_i, M_i = 1) P(M_i^{\text{obs}} | N_i^{\text{obs}}, \theta_i, M_i = 1) \quad (6b)$$

$$+ (1 - \delta_i) P(N_i^{\text{obs}} | \theta_i, M_i = 0) P(M_i^{\text{obs}} | N_i^{\text{obs}}, \theta_i, M_i = 0), \quad (6c)$$

and so the log posterior distribution of the parameters $\theta = (\theta_1, \dots, \theta_n)$, $\delta = (\delta_1, \dots, \delta_n)$ for all the data $\mathbf{x} = ((N_1^{\text{obs}}, M_1^{\text{obs}}), \dots, (N_n^{\text{obs}}, M_n^{\text{obs}}))$ under our model is 186
187

$$\log f(\theta, \delta | \mathbf{x}) \propto \sum_{i=1}^n \left(\log P(N_i^{\text{obs}}, M_i^{\text{obs}} | \theta_i, \delta_i) + \log f(\theta_i, \delta_i) \right), \quad (7)$$

where we use f to denote posterior and prior densities. 188

2.4.2 Base model prior densities 189

In the base model, we modelled the individual-level probability of multiple infection not conditional on the observed data as identical for all i with a prior density with diffuse variance [57]: 190
191

$$\text{logit}(\delta_i) = \delta_0 \sim \text{Normal}(0, 3.16^2). \quad (8)$$

Given the log-linear dependency of sequencing success on log viral viral load [33], known differences in sequencing success rates by sampling protocol [38], and other factors, we specified the prior on the individual-level sequencing probability θ_i through a logistic mixed effects model. Specifically, we modeled $\text{logit}(\theta_i)$ with

$$\begin{aligned}\text{logit}(\theta_i) &= \alpha_0 + \alpha^{\text{bait}} X_i^{\text{bait}} \\ &\quad + \alpha^{\text{amplicon-vl}} V_i^a X_i^{\text{amplicon}} + \alpha^{\text{bait-vl}} V_i^b X_i^{\text{bait-capture}} + \alpha_i \\ \alpha_0 &\sim \text{Normal}(0, 2^2) \\ \alpha^{\text{bait}} &\sim \text{Normal}(0, 2^2) \\ \alpha^{\text{amplicon-vl}}, \alpha^{\text{bait-capture-vl}} &\sim \text{Normal}(0, 2^2), \\ \alpha_i &\sim \text{Normal}(0, \sigma_\alpha^2) \\ \sigma_\alpha &\sim \text{Half-Cauchy}(0, 1)\end{aligned}\tag{9}$$

where X_i^{amplicon} and X_i^{bait} are indicator variables for whether sample i was sequenced using the amplicon or bait capture approach respectively, and V_i^a and V_i^b were the \log_{10} copies/mL values for amplicon and bait capture sequenced samples, respectively, standardized to have mean zero and standard deviation 1, and α_i denotes an individual-level random effect.

2.4.3 Modelling false-negative and false-positive phylogenetic observations

We extended the base model to account for possible false-negative and false-positive phylogenetic observations, accounting for incomplete removal of false-positive observations through *phyloscanner*, and/or incomplete phylogenetic identification of multiple infections due to insufficient phylogenetic background. First, among individuals in which $M_i = 1$ we accounted for the scenario in which both variants are successfully sequenced in a given window but were identified as a single phylogenetic clade by *phyloscanner*, i.e. false-negative observations, by modifying our data generating model (Eq 2) to

$$(M_i^{\text{obs}} | N_i^{\text{obs}}, \theta_i, M_i = 1) \sim \text{Binomial}\left(N_i^{\text{obs}}, \frac{\theta_i}{2 - \theta_i} (1 - \lambda)\right),\tag{10}$$

where λ represents the false-negative rate. We analogously accounted for the scenario in which only a single variant was sequenced but *phyloscanner* spuriously assigned multiple subgraphs in a given window, i.e. false-positive observations, through a false-positive rate ϵ in the model. We modeled false-positives among samples lacking multiple infection and among windows in multiply infected samples in which only a single variant was sequenced, which occurs with probability $2\frac{1-\theta_i}{2-\theta_i}$ when $N_{i,w} = 1$, but was spuriously assigned to two subgraphs. Note that because we did not differentiate between windows with exactly 2 and > 2 subgraphs, we do not consider the scenario where both variants are sequenced in a true multiple infection and the two sequenced variants are spuriously assigned to 3 or 4 subgraphs. Our data generating model (Eq 3b) was updated to account for false-positives and false-negatives as:

$$(M_i^{\text{obs}} | N_i^{\text{obs}}, \theta_i, M_i = 1) \sim \text{Binomial}\left(N_i^{\text{obs}}, \frac{\theta_i}{2 - \theta_i} (1 - \lambda) + 2\epsilon \frac{1 - \theta_i}{2 - \theta_i}\right)\tag{11a}$$

$$(M_i^{\text{obs}} | N_i^{\text{obs}}, \theta_i, M_i = 0) \sim \text{Binomial}(N_i^{\text{obs}}, \epsilon),\tag{11b}$$

with additional prior densities

$$\text{logit}(\lambda) \sim \text{Normal}(0, 1)\tag{12a}$$

$$\text{logit}(\epsilon) \sim \text{Normal}(0, 1),\tag{12b}$$

and all other components of the model remaining as above.

2.4.4 Estimating risk factors of multiple infection

We further extended the model described above to model the probability of multiple infection as dependent on potential clinical, behavioral, and/or epidemiological risk factors through a logistic regression approach.

Specifically, we modeled the logit of the individual-level multiple infection prior probabilities (Eq 8) as a linear predictor of fixed effects and associated Horseshoe-type shrinkage priors [58,59] on the effect sizes to handle correlated individual-level covariates,

$$\text{logit}(\delta_i) = \delta_0 + X_i^{\text{risk}} \beta \quad (13a)$$

$$(\beta_j | \xi_j, \tau) \sim \text{Normal}(0, \xi_j^2 \tau^2) \quad (13b)$$

$$\xi_j \sim \text{Half-}t_2(0, 1) \quad (13c)$$

$$\tau \sim \text{Half-Cauchy}(0, 1), \quad (13d)$$

where X_i^{risk} is a $1 \times j$ dimensional row vector of multiple infection predictive covariates and β is a $p \times 1$ dimensional column vector of fixed effect coefficients. We also considered fixed effects models without variable selection in sensitivity analysis with $\beta \sim N(0, 1)$. As above, the number of lifetime sex partners included missing and ambiguous responses (e.g. “3+”), and these values were estimated as additional random variables in the Bayesian inference, assuming they were missing at random within sex, age, and community type, using lognormal prior distributions specific to these strata defined by the non-missing responses (Materials and methods). Imputed values for missing responses were limited to the range [1,60] and responses of “3+” were limited to the range [3,60].

2.4.5 Parameter estimation

We estimated the posterior distribution of all parameters in these models using Hamiltonian Monte Carlo [60] with the No-U-Turn Sampler [61] implemented in Stan [57] and accessed through cmdStanR v.2.31.0 [62] in R. For all analyses, four independent chains with 500 iterations of warm up and 2000 iterations of sampling were run. A target acceptance rate of 0.8 was used for all analyses with the exception of those that employed shrinkage priors where a target acceptance rate of 0.95 was used to avoid divergent transitions. Convergence was assessed using the \hat{R} statistic, bulk and tail effective sample sizes (ESS) for each parameter [63], and visual inspection of trace and pairs plots (S4 File).

2.4.6 Generated quantities

Based on the estimated parameter distributions of the models described above, we generated a number of quantities to aid in interpretation of our results.

2.4.6.1 Expected number of multiple subgraph windows Under the base model definition with no false-positives or false-negatives (Eq 2), we calculated an expected value for θ_i and consequently $(M_i^{\text{obs}} | M_i = 1)$ given an observed value for N_i^{obs} :

$$E[\theta_i | N_i^{\text{obs}}, M_i = 1] = 1 - \sqrt{1 - \frac{N_i^{\text{obs}}}{n^{\text{max}}}} \quad (14)$$

$$E[M_i^{\text{obs}} | \theta_i, M_i = 1] = n^{\text{max}} \theta_i^2. \quad (15)$$

2.4.6.2 Individual posterior probability of multiple infection Based on the latent-class finite mixture model described above (Eq 7), the probability that any given sequenced participant i harbors a multiple infection conditional the observed data and all parameters is:

$$P(M_i = 1 | N_i^{\text{obs}}, M_i^{\text{obs}}, n^{\text{max}}, \theta_i, \delta_i, \lambda, \epsilon) = \frac{P(N_i^{\text{obs}}, M_i^{\text{obs}} | n^{\text{max}}, \theta_i, \lambda, \epsilon, M_i = 1) \delta_i}{P(N_i^{\text{obs}}, M_i^{\text{obs}} | n^{\text{max}}, \theta_i, \delta_i, \lambda, \epsilon)}. \quad (16)$$

The target quantity can therefore be obtained by integrating over unknown parameters:

$$P(M_i = 1 | N_i^{\text{obs}}, M_i^{\text{obs}}, n^{\text{max}}) = \int P(M_i = 1 | N_i^{\text{obs}}, M_i^{\text{obs}}, n^{\text{max}}, \theta_i, \delta_i, \lambda, \epsilon) P(\theta_i, \delta_i, \lambda | N_i^{\text{obs}}, M_i^{\text{obs}}) d\theta_i d\delta_i d\lambda, \quad (17)$$

which we approximated by taking Monte Carlo samples of $P(M_i = 1 | N_i^{\text{obs}}, M_i^{\text{obs}}, n^{\text{max}}, \theta_i, \delta_i, \lambda, \epsilon)$.

2.4.6.3 Prevalence of multiple infection among sequenced participants Under the base model (Eq 8), the posterior estimate of the prevalence of multiple infection in the study sample is given by:

$$\bar{\delta} = \text{inverse-logit}(\delta_0) = \frac{\exp(\delta_0)}{1 + \exp(\delta_0)}. \quad (18)$$

In the presence of modeled risk factors, the prevalence of multiple infections among sequenced participants will vary based on sub-groups s defined by X^{risk} :

$$\bar{\delta}_{i \in s} = \text{inverse-logit}(\delta_0 + X_{i \in s}^{\text{risk}} \beta). \quad (19)$$

2.4.6.4 Risk ratio of harboring multiple infection associated with epidemiological covariates

Finally, we calculated the risk ratio for harboring a multiple infection associated with being in epidemiological strata $s = S^*$ as compared to strata $s = S$ by first calculating the risk of multiple infection in S^* and S ($\bar{\delta}_{S^*}$ and $\bar{\delta}_S$, respectively) as above (Eq 19). The risk ratio was therefore calculated as:

$$\text{RR}^{S^*, S} = \frac{\bar{\delta}_{i \in S^*}}{\bar{\delta}_{i \in S}}. \quad (20)$$

2.5 Simulation study

We used simulations to validate our inference model. For all simulations, we simulated data for $n^{\text{max}} = 29$ genome windows in $N = 2,000$ samples which were assigned a normalized \log_{10} viral load (V_i) with random draws from a $N(0, 1)$ distribution. For all samples, α_i was drawn from a $N(0, 1)$ distribution and θ_i calculated as $\alpha_0 + \alpha_1 V_i + \alpha_i$ with $\alpha_0 = 2$ and $\alpha_1 = 2$. Under these parameters, we generated three simulated data sets as described below.

2.5.1 Base simulation

$$M_i = [1 \times 100] \oplus [0 \times 1900] \quad (21a)$$

$$(N_i^{\text{obs}} | M_i = 0) \sim \text{Binomial}^{1+}(29, \phi_i) \quad (21b)$$

$$(N_i^{\text{obs}} | M_i = 1) \sim \text{Binomial}^{1+}(29, (1 - (1 - \phi_i)^2)) \quad (21c)$$

$$(M_i^{\text{obs}} | M_i = 0) \sim \text{Binom}(N_i^{\text{obs}}, 0) \quad (21d)$$

$$(M_i^{\text{obs}} | M_i = 1) \sim \text{Binomial}\left(N_i^{\text{obs}}, \frac{\phi_i}{2 - \phi_i}\right), \quad (21e)$$

where $[x \times n]$ represents a vector of x repeated n times and \oplus represents concatenation of two vectors.

2.5.2 Full simulation

$$M_i = [1 \times 100] \oplus [0 \times 2000] \quad (22a)$$

$$(N_i^{\text{obs}} | M_i = 0) \sim \text{Binomial}^{1+}(29, \phi_i) \quad (22b)$$

$$(N_i^{\text{obs}} | M_i = 1) \sim \text{Binomial}^{1+}(29, (1 - (1 - \phi_i)^2)) \quad (22c)$$

$$(M_i^{\text{obs}} | M_i = 0) \sim \text{Binom}(N_i^{\text{obs}}, \epsilon) \quad (22d)$$

$$(M_i^{\text{obs}} | M_i = 1) \sim \text{Binom}\left(N_i^{\text{obs}}, \frac{\phi_i}{2 - \phi_i}(1 - \lambda) + 2\epsilon \frac{1 - \phi_i}{2 - \phi_i}\right) \quad (22e)$$

$$\lambda = 0.30 \quad (22f)$$

$$\epsilon = 0.01. \quad (22g)$$

Additional simulations from this simulation model were generated with all other parameters held constant except (A): $\sum_i^n M_i = 0, 300, 600$, (B): $\lambda = 0.10, 0.20, 0.40$, and (C): $\epsilon = 0, 0.005, 0.05$.

2.5.3 Extended simulation

253

$$M_i = [1 \times 150] \oplus [0 \times 1850] \quad (23a)$$

$$X_{,1} = [1 \times 100] \oplus [0 \times 50] \oplus [1 \times 900] \oplus [0 \times 950] \quad (23b)$$

$$X_{i,2-5}^{\text{risk}} \sim \text{shuffle}([1 \times 1000] \oplus [0 \times 1000]) \quad (23c)$$

$$(N_i^{\text{obs}} | M_i = 0) \sim \text{Binomial}^{1+}(29, \phi_i) \quad (23d)$$

$$(N_i^{\text{obs}} | M_i = 1) \sim \text{Binomial}^{1+}(29, (1 - (1 - \phi_i)^2)) \quad (23e)$$

$$(M_i^{\text{obs}} | M_i = 0) \sim \text{Binomial}(N_i^{\text{obs}}, \epsilon) \quad (23f)$$

$$(M_i^{\text{obs}} | M_i = 1) \sim \text{Binomial}\left(N_i^{\text{obs}}, \frac{\phi_i}{2 - \phi_i}(1 - \lambda) + 2\epsilon \frac{1 - \phi_i}{2 - \phi_i}\right), \quad (23g)$$

where $X_{i,j}^{\text{risk}}$ represents the entry in the i th row and j th column of the design matrix X^{risk} and $\text{shuffle}(v)$ denotes shuffling the elements of v .

254

255

2.6 Data analysis and visualization

256

All data analysis was conducted in R v.4.4.1 [64] using the tidyverse [65] with dplyr v.1.1.4 [66], tibble v.3.2.1 [67], and tidyr v.1.3.1 [68]. Haven v.2.5.4 [69] was used to parse a subset of input data files. Visualization of data and results was done using ggplot2 v.3.5.1 [70] with bayesplot v.1.11.1 [71, 72], cowplot v.1.1.3 [73], and patchwork v.1.2.0. [74]. Phylogenetic trees were manipulated and visualized using ape v.5.8 [75], ggtree v.3.12.0 [76–80], phytools v.2.1.1 [81], and tidytree v.0.4.6 [76]. Highest posterior density intervals were calculated with HDInterval v.0.2.4 [82] and convergence statistics were assessed with posterior v.1.6.0 [83]. Preliminary analyses and model fitting was performed using fitdistrplus v.1.1-11 [84].

257

258

259

260

261

262

263

2.7 Data and code availability

264

Processed *phyloscanner* output, de-identified epidemiological metadata, and all analysis and visualization code is available at https://github.com/m-a-martin/rccs_hiv_moi. HIV consensus sequences are available from Zenodo (<https://doi.org/10.5281/zenodo.10075814>) and the PANGAEA-HIV sequence repository (<https://github.com/PANGAEA-HIV/PANGAEA-Sequences>) as open-access dataset under the CC-BY-4.0 license [85].

265

266

267

268

269

HIV-1 deep-sequence reads can be requested from PANGAEA-HIV under a managed access policy due to privacy and ethical reasons, which aligns with UNAIDS ethical guidelines. The process for accessing data, the PANGAEA-HIV data sharing policy and a detailed description of what data are available is described at <https://www.pangea-hiv.org/join-us>. For more information contact PANGAEA project manager Lucie Abeler-Dörner (lucie.abeler-dorner@ndm.ox.ac.uk). The time frame for a response to requests is 2–4 weeks.

270

271

272

273

274

Additional cohort data can be requested from RHSP. Because of privacy and ethical reasons, RHSP maintains a controlled access data policy for corresponding epidemiological metadata and corresponding data collection tools. In brief, RHSP policy requires individuals to submit an RHSP data request form (available upon request from info@rhsp.org or gkigozi@rhsp.org) and a brief concept note (one or two pages) detailing their research questions and methods. In addition, researchers are asked to provide a curriculum vitae/resume along with proof of human subjects research training. The time frame for a response to requests is 2–4 weeks.

275

276

277

278

279

280

3 Results

281

3.1 Phylogenetic signatures of multiple infection in population-based pathogen surveillance

282

283

Between 2010 and 2020, 50,967 participants contributed to the RCCS in 109,608 visits over six survey rounds. Overall, 8,841 participants were HIV seropositive and 3,586 were viremic (plasma viral load $\geq 1,000$ copies/mL) at one of their visits. Among these participants with viremic HIV, 2,029 sampled between October 2010 and May 2019 had available HIV deep-sequence data at minimum quality criteria for deep-sequence

284

285

286

287

phylogenetic analysis and were identified as a member of a putative transmission network (Table 1 and S1 File). Availability of sequence data among viremic participants was generally higher among men, from residents of fishing communities, and from participants aged 25-34 years.

We next inferred within-host phylogenies from deep-sequencing reads in twenty-nine 250 bp non-overlapping genomic windows using *phyloscanner* (S5 File), which captured evolutionary relationships of HIV variants within individual participants. Sequencing coverage varied significantly between samples (median [interquartile range (IQR)]: 5000 [4250] bp, S1 FigA) but was generally higher among bait capture sequenced samples and samples with higher viral load. Across the genome, sequencing success was highest in *gag* (Fig 1F, S1 FigB), likely due to differential amplification efficiency of the primers used in the amplicon sequencing approach [86].

Table 1. Characteristics of the study sample obtained from population-level HIV deep-sequence surveillance in the Rakai Community Cohort Study, 2010-2020, stratified by availability of deep-sequence data.

	Participants living with HIV			
	All	Viremic	Processed w/ PHSC <i>n</i> (%)	% of viremic (95% CI)
Overall	8,841	3,586	2,029	
Survey Round				
2010	1,812 (21.72%)	35 (1.11%)	16 (0.79%)	45.71% (30.46% - 61.82%)
2012	2,202 (26.4%)	992 (31.58%)	749 (36.91%)	75.5% (72.73% - 78.08%)
2014	1,170 (14.03%)	653 (20.79%)	346 (17.05%)	52.99% (49.15% - 56.79%)
2015	1,292 (15.49%)	727 (23.15%)	523 (25.78%)	71.94% (68.56% - 75.09%)
2017	1,080 (12.95%)	511 (16.27%)	328 (16.17%)	64.19% (59.94% - 68.23%)
2019	786 (9.42%)	223 (7.1%)	67 (3.3%)	30.04% (24.4% - 36.37%)
Sex				
Female	5,315 (63.71%)	1,685 (53.65%)	1,032 (50.86%)	61.25% (58.9% - 63.54%)
Male	3,027 (36.29%)	1,456 (46.35%)	997 (49.14%)	68.48% (66.04% - 70.81%)
Community type				
Inland	4,974 (59.63%)	1,212 (38.59%)	742 (36.57%)	61.22% (58.45% - 63.92%)
Fishing	3,368 (40.37%)	1,929 (61.41%)	1,287 (63.43%)	66.72% (64.58% - 68.79%)
Age				
(14, 24]	1,472 (17.65%)	678 (21.59%)	431 (21.24%)	63.57% (59.88% - 67.11%)
(24, 34]	1,472 (17.65%)	678 (21.59%)	1,052 (51.85%)	66.71% (64.34% - 68.99%)
(34, 49]	2,995 (35.9%)	886 (28.21%)	546 (26.91%)	61.63% (58.38% - 64.77%)
Viral load (log ₁₀ copies/mL)				
(3, 3.5]		466 (14.84%)	275 (13.55%)	59.01% (54.49% - 63.39%)
(3.5, 4]		803 (25.57%)	522 (25.73%)	65.01% (61.64% - 68.23%)
(4, 4.5]		806 (25.66%)	521 (25.68%)	64.64% (61.28% - 67.86%)
(4.5, 5]		661 (21.04%)	447 (22.03%)	67.62% (63.96% - 71.08%)
(5, ∞]		405 (12.89%)	264 (13.01%)	65.19% (60.42% - 69.66%)

For each participant, includes data from the participant-visit processed with PHSC if applicable or the participant-visit with the highest viral load, using the first visit in the case of ties or for people not living with HIV. Viremic participants excludes individuals living with HIV with suppressed viral load or missing viral load data. Viral load testing was not routinely conducted in earlier study rounds and was available for 37.32% of participant-visits contributed by people living with HIV in the 2010 and 2012 rounds. In recent rounds, viral load testing is routinely conducted and is available for 99.67% of participant-visits contributed by people living with HIV in the 2014- 2019 surveys. Percentages represent the row percentages within each category. Binomial confidence intervals were calculated using the Agresti–Coull method. PHSC = phyloscanner.

To characterise phylogenetic signatures of multiple infection, *phyloscanner* was used to identify distinct co-circulating variants among participants with viremic HIV (Materials and methods and Fig 1A,B). We tabulated the number (M_i^{obs}) of genome windows in which distinct phylogenetic lineages (phylogenetic

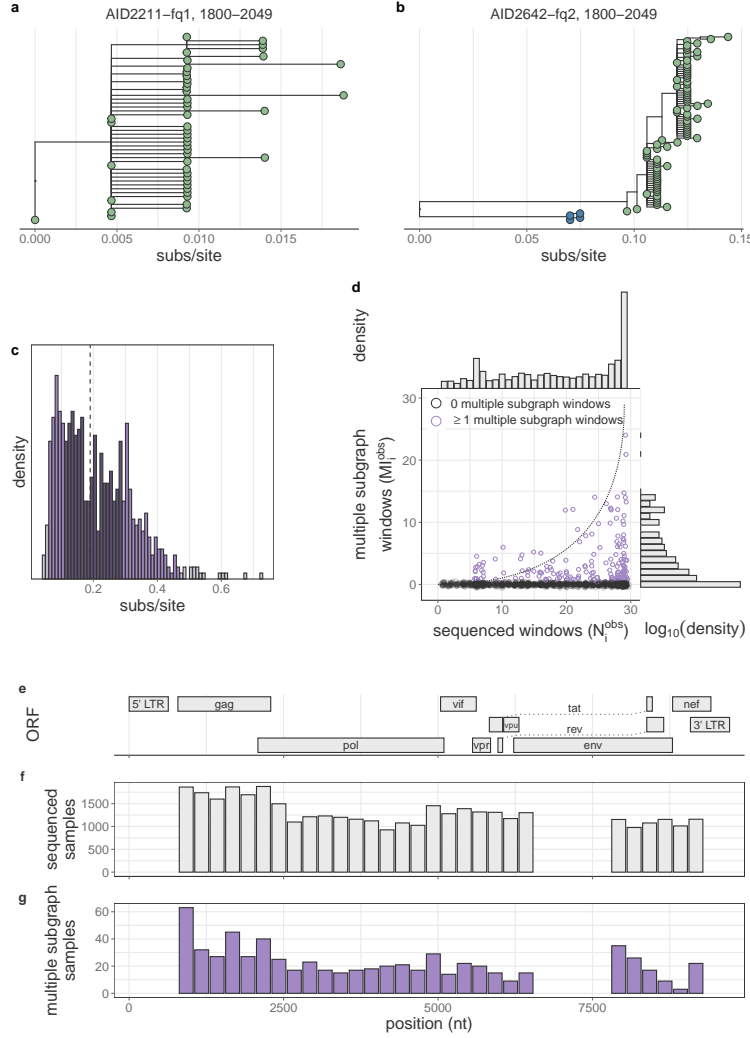


Fig 1. Empiric phylogenetic multiple infection signatures from 2,029 samples from people with viremic HIV in the Rakai Community Cohort Study, 2010-2020. (A) Representative within-host phylogenetic tree lacking evidence of multiple phylogenetic subgraphs. (B) Representative within-host phylogenetic tree with two subgraphs as indicated by the green and blue shading of the tips. (C) Distribution of branch length distance between the MRCA of the two subgraphs with the most sequencing reads in all genome windows with ≥ 2 subgraphs from all samples. Bins are shaded according to the 95th and 50th percentile. Vertical dotted line indicates median value. Binwidth is calculated such that there are approximately 50 bins across the range of observed values. (D) Per-sample number of non-overlapping genome windows with sequence data versus the number of non-overlapping genome windows with multiple subgraphs. Samples with at least one window with multiple subgraphs are shown in purple. Points have been jittered along both the X and Y axes for visual clarity. Dotted line shows modeled prediction in the absence of false-positive or false-negative multiple subgraph windows. Marginal densities are shown at right and above the scatter-plot. (E) Schematic of the HIV genome based on the coordinates from HXB2 (Genbank: K03455.1). (F) Number of samples with sequence data in each of the 29 non-overlapping genome windows. (G) Number of samples with evidence of multiple subgraphs in each of the 29 non-overlapping genome-windows.

subgraphs) were observed. The median genetic distance between the most recent common ancestors of subgraphs in genome windows with multiple subgraphs was 0.19 [IQR: 0.17] substitutions/site (Fig 1C), which is consistent with the circulating genetic diversity within Rakai [9, 55] and comparable to HIV inter-subtype

genetic distances [87]. In total, 180 (8.87%) samples had multiple subgraphs in at least one of the 29 non-overlapping windows (Fig 1D). Among these, the proportion of sequenced windows in which multiple subgraphs were observed varied considerably, but was generally relatively rare (median [IQR] 11.11 [19.14]%, 2 [3] windows). We further observed a clear dependence of the ability to identify multiple subgraphs on sequencing success as quantified by genome coverage in the *phyloscanner* output. Of those samples with sequence data in all genome windows, 12.26% (52/424) had at least one window with multiple subgraphs compared to 7.98% (128 / 1605) among the remaining samples. Multiple subgraph windows were more common in the genome windows corresponding to *gag*, *env*, and *nef*, likely reflecting circulating genetic diversity in these regions with higher substitution rates [88].

3.2 Bayesian model to identify multiple infections from pathogen deep-sequence data

The observed dependence between phylogenetically identified samples with multiple infection and successful genome sequencing implies it is difficult to deduce the underlying prevalence of multiple infections from the empirical data without a statistical model that accounts for partial sequencing success, false-positive multiple subgraphs, and false-negative unique subgraphs within hosts. Specifically, because identification of multiple infection requires successful sequencing of both variants and genetic divergence between those variants, there is inherently more uncertainty in multiple infection status when sequencing success is poor or when infecting variants are genetically related in the sequenced region of the genome. Further, contamination or sequencing errors giving rise to spurious within-host genetic diversity will inflate estimates rates of multiple infection.

Therefore, we constructed a Bayesian model accounting for partial sequencing success to estimate the probabilities that each individual harbors a multiple infection, prevalence of multiple infection among deep-sequenced viremic participants, and risk factors for multiple infection (Materials and methods). We first verified that we were able to accurately estimate model parameters on simulated test data in the presence of incomplete sequencing success (S4 Table). Next, we investigated the impact of false-positive and false-negative observations, as empiric analyses of RCCS deep-sequence data indicated that false-negative rates were likely substantial in that among samples with $M_i^{\text{obs}} > 0$, the observed M_i^{obs} values for a given number of sequenced windows (N_i^{obs}) was less than expected based on our model (Eq 15 and Fig 1D). We found that failing to account for these errors led to an overestimation of the prevalence of multiple infections on simulated data (Fig 2A and S5 Table). This prompted us to explicitly include false-positive and false-negative detection rates in our model as free parameters (Eq 11). With this, we found that model parameters could be accurately estimated on simulated data (Fig 2B-H and S6 Table). Model performance was robust across simulations covering a range of reasonable values of the prevalence of multiple infections as well as false-positive and false-negative rates of multiple subgraph observation (S2 Fig, S3 Fig, and S4 Fig).

To identify risk factors for multiple infection among people living with HIV, we formulated an extended model in which individual-level prior multiple infection probabilities are described with a logit linear predictor of putative risk factors (Eq 13). On simulated data, this model accurately estimated the true risk ratio associated with a covariate leading to a two-fold higher probability of harboring a multiple infection (risk ratio (RR) median [95% HPD] 1.74 [1.07 - 2.47]) in the context of four additional background null covariates (S7 Table).

3.3 Prevalence of HIV multiple infections among sequenced participants

Of the 2,029 participants living with viremic HIV, 94 (4.63%) had a median posterior probability of multiple infection greater than 50% (Fig 3A,B). Our empirical analyses above demonstrated that the number of genome windows with multiple subgraphs is less than would be expected in the absence of false-negatives (Fig 1). In line with this observation, the model estimated a high false-negative rate (median [95% HPD] 57.18% [52.94% - 61.6%], S8 Table), implying that empirical phylogenetic signatures of multiple infection under-estimate the true infection status of individuals in any single HIV genomic windows. It was therefore essential to have whole-genome data from a subset of participants (Fig 1) to estimate false-negative detection rates. Further, informed by the 91.13% of samples with no multiple subgraph windows, we estimated the false-positive rate to be low (0.32% [0.25% - 0.4%]). However, we note that even a low absolute rate may give rise to a considerable number of samples with multiple subgraph windows in the absence of multiple infections.

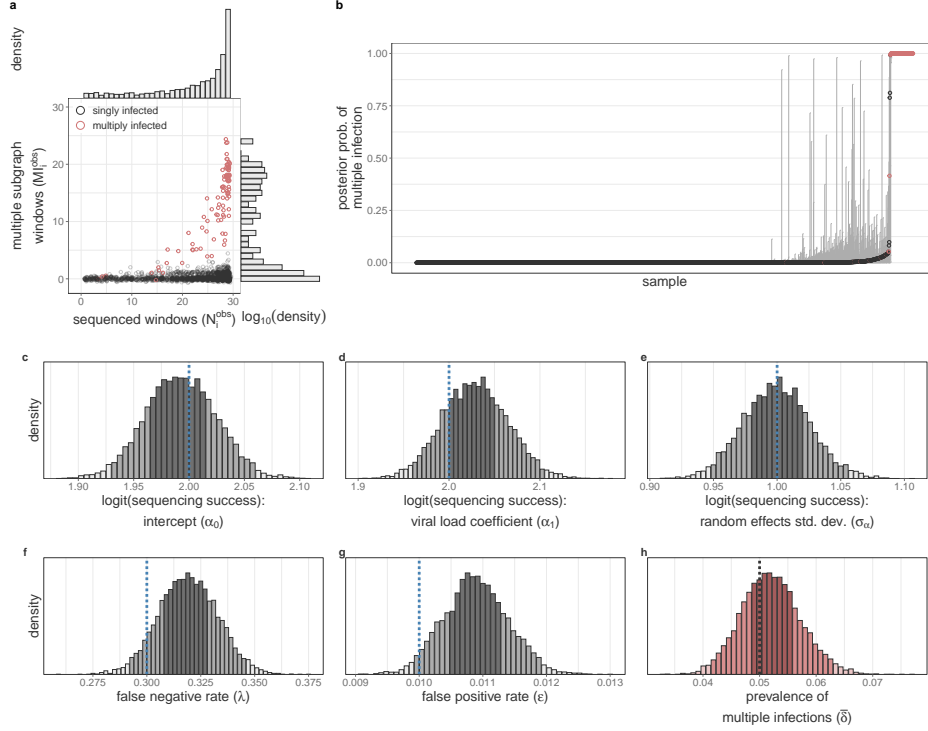


Fig 2. Verification of model accuracy for estimating multiple infection prevalence on simulated data with incomplete sequencing success and false-negative and false-positive observations. (A) Number of windows with sequence data (x-axis) v. number of windows with multiple subgraphs (y-axis) for each simulated sample. Data from multiply infected samples is highlighted in red. Marginal distributions are shown at right and above. (B) Estimated posterior probability of multiple infection for each sample. Confidence bounds represent the 95% highest posterior density. Data for each sample is shaded as in (A). (C-H) Posterior distributions of the baseline sequencing success (α_0 , C), dependence of sequencing success on viral load (\log_{10} copies/mL) standardized to mean = 0 and standard deviation = 1. (α_1 , D), standard deviation of per-individual sequencing success random effect (σ_α , E), the multiple subgraph false-negative rate (λ , F), the multiple subgraph false-positive rate (ϵ , G), and the population prevalence of multiple infections (δ , H). Posterior distributions in (C-H) bins are shaded according to the 95% and 50% HPD. Histogram bin width is calculated such that there are approximately 50 bins over the range of the plotted values. True values are shown as vertical dotted lines.

Accounting for false-positive and false-negative rates, the estimated prevalence of multiple infections in the sequenced sample was 5.79% [4.56% - 7.07%] (Fig 3B and S8 Table).

We next used our model to identify individuals with phylogenetically likely multiple infection. Classification was based on the inferred, posterior multiple infection probabilities, and therefore our model-based approach accounted for individual-level factors associated with sequencing success and population-level false-positive and false-negative rates (Eq 17). We determined a binary classification cut-off above which individuals were classified as having a phylogenetically likely multiple infection such that the total number of identified individuals was consistent with the estimated prevalence in the sample, resulting in a cut-off of 3.1%. Using this threshold, we identified 117 individuals with a likely multiple infection (Fig 3B).

3.4 Risk factors of HIV multiple infection

In African contexts, HIV infection risk varies at the individual-level, such as by age, gender, sexual behaviour and circumcision status, and at the community-level [35, 36, 40]. We therefore next aimed to characterize individual and population-level risk factors for multiple infection with HIV. First, given the significantly higher prevalence of HIV and viremic HIV in Lake Victoria fishing communities [36, 89], we investigated

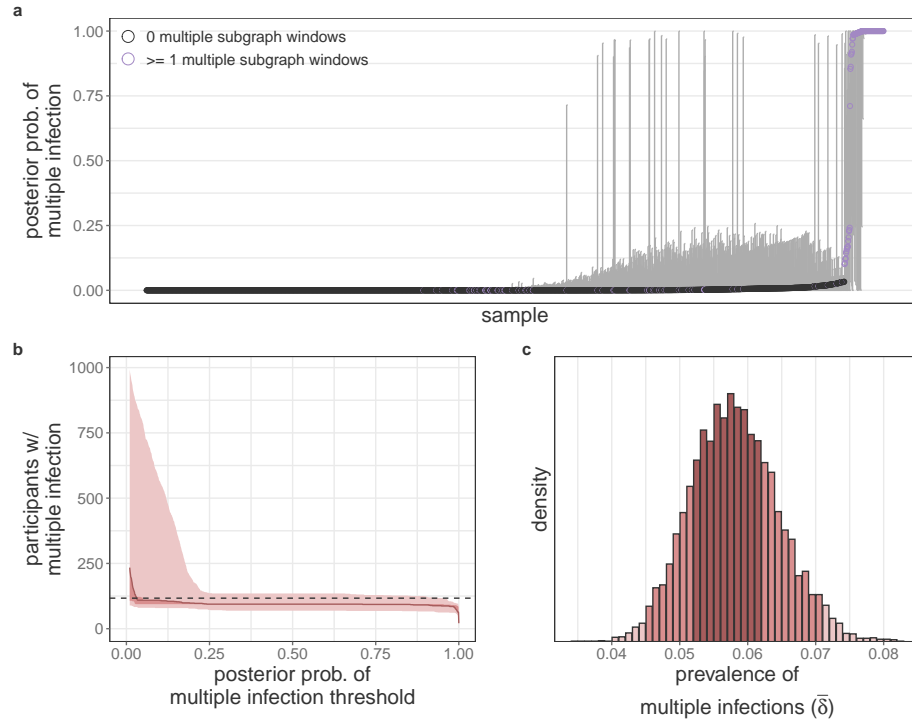


Fig 3. Individual-level estimates and population-level characteristics of HIV multiple infection in people with viremic HIV in the Rakai Community Cohort Study, 2010-2020. (A) Estimated posterior probability of multiple infection for each participant. Confidence bounds represent the 95% highest posterior density. Participants with at least one multiple subgraph window are shown in purple. (B) Number of participants with multiple infection as a function of the threshold used to dichotomize the probability of multiple infection. Central estimate uses the median estimated prevalence of multiple infections and shading uses 95% and 50% HPD. Horizontal dotted line plotted at the number of participants needed to match the estimated population prevalence of multiple infection. (C) Posterior distribution of the prevalence of multiple infections among sequenced viremic participants in the RCCS. Bins are shaded according to the 95% and 50% HPD. Histogram width is calculated such that there are approximately 50 bins over the range of the plotted values.

whether participants with viremic HIV in these communities had increased risk of multiple infection as compared to participants with viremic HIV in inland communities. We additionally incorporated a binary feature describing the sequencing technology used to generate the deep-sequence data from each participant to assess the extent of technical bias in our inferences. In this two-feature model with diffuse priors on the effect sizes, we indeed found that the risk of prevalent multiple infection in participants with viremic HIV in fishing communities was 2.04 times (95% HPD 1.15 - 3.22) greater than in inland communities (with posterior median [95% HPD] prevalence of multiple infection of 8.32% [6.11% - 10.96%]) and 4.05% [2.24% - 6.31%] respectively, Fig 4A and S9 Table). The estimated risk ratio for HIV multiple infection was therefore broadly comparable to the risk ratio of HIV prevalence and viremia in fishing as compared to inland communities (2.5-3) [36, 89], consistent with the expectation that the risk of superinfection acquisition scales with the population prevalence of viremic HIV.

In a univariate analysis, we estimated that multiple infections were less common among participants sequenced using the bait-approach protocol (RR median [95% HPD]: 0.65 [0.42 - 0.94], S10 Table). However, 50.45% of bait-capture sequenced participants were residents of fishing communities compared to 76.02% of amplicon sequenced participants. Consequently, after accounting for community type, the estimated magnitude of the dependence of multiple infection status on sequencing technology was considerably reduced and no longer considered to be significant (RR [95% HPD] 0.76 [0.47 - 1.1], S9 Table).

Participants with HIV in fishing communities also reported having more lifetime sex partners (S5 Fig), so

we next assessed whether the risk of harboring a multiple infection differed by the number of self-reported lifetime sex partners within each of the two community locations. As women tend to under-report their number of sex partners relative to men [90], we restricted this analysis to male participants. The number of lifetime sexual partners generally increases with age, and so we standardized responses relative to the age-specific mean number of lifetime sexual partners among participants separately for the inland and fishing communities (S6 Fig). Among 997 male participants included in this analysis, 516 reported an exact number of lifetime sex partners, 477 responded they had three or more lifetime partners, and 4 did not provide a response. We imputed ambiguous responses and missing data within our inference framework by assuming responses were missing at random between people with and without multiple infection (Materials and methods).

We did not find a statistically significantly higher risk of multiple infection in male participants with more lifetime sexual partners in the context of substantial missing data and sampling over potential missing values using age-specific prior distributions. However, we note that the posterior effect size translated into an estimated more than two-fold higher risk of multiple infection between men living with viremic HIV in fishing communities associated with having 30 lifetime sexual partners compared to one lifetime sexual partner (e.g. RR [95% HPD] among 25-29 year olds 2.39 [0.59 - 5.37], Fig 4B and S7 Fig for all age groups). Very similar results were observed using a complete case analysis of the 516 men who provided an exact number of lifetime sex partners (S12 Table).

We also performed a comprehensive discovery-based risk factor variable selection analysis over eight additive biological, behavioral and epidemic features, stratifying epidemiological and behavioral variables by community type to account demographic differences between the populations and excluding additional variable interactions. This analysis confirmed residency in fishing communities as a risk factor (multivariate RR [95% HPD] 2.49 [0.12 - 7.63]), but did not identify any other variables that were associated with significantly higher or lower risk of multiple infection in our sample (Fig 4C and S13 Table). Specifically, despite the fact that female bar/restaurant workers face a three-fold higher risk of incident HIV [40] we did not identify an increased risk of multiple infection among female bar/restaurant workers or men who have sex with bar/restaurant workers in either inland or fishing communities.

4 Discussion

In this large-scale study, we assessed the prevalence and risk factors of HIV multiple infection in an East African setting with high HIV burden using population-based pathogen deep-sequence surveillance data. To do this, we developed a Bayesian statistical model to identify multiple infections in deep-sequence phylogenies such as those generated by *phyloscanner* [37]. Our model incorporates false-negative and false-positive rates for the presence of genetically distinct viral lineages and simultaneously estimates individual and population-level probabilities of harboring multiple infection. This framework also allows for the identification of biological and epidemiological risk factors for harboring a multiple infection. In simulation analyses, we demonstrated the ability of the model to generate accurate inferences across a range of parameter values and fit the model to *phyloscanner* within-host phylogenies inferred from whole-genome deep-sequence data from 2,029 viremic participants in the Rakai Community Cohort Study, a population-based open-cohort in southern Uganda. We estimated that the cross-sectional prevalence of simultaneous multiple infections among sequenced viremic participants in this cohort is approximately 6%. Further, we showed that viremic participants with HIV living in high HIV prevalence fishing communities along Lake Victoria were more than twice as likely to harbor a multiple infection as compared to those living in inland agrarian or trading communities. Among male residents in fishing communities, we estimated that those with more lifetime sex partners can be expected to be more likely to have a multiple infection, although this finding did not reach statistical significance at the 95% level.

This study represents the largest analysis of HIV multiple infections by more than an order of magnitude [19] and the first to rigorously account for partial sequencing success and uncertainty in individual-level estimates when estimating population-level risk of multiple infection. Our model indicated that in the context of incomplete genome coverage, as is common in HIV whole-genome sequencing [33], evidence for multiple infections is expected to be observed in only a subset of genome windows. However, we observed a high rate of false-negatives beyond what is expected due to incomplete sequencing, which may be due to insufficient diversity of infecting lineages in some regions of the genome [88] to phylogenetically distinguish them. This

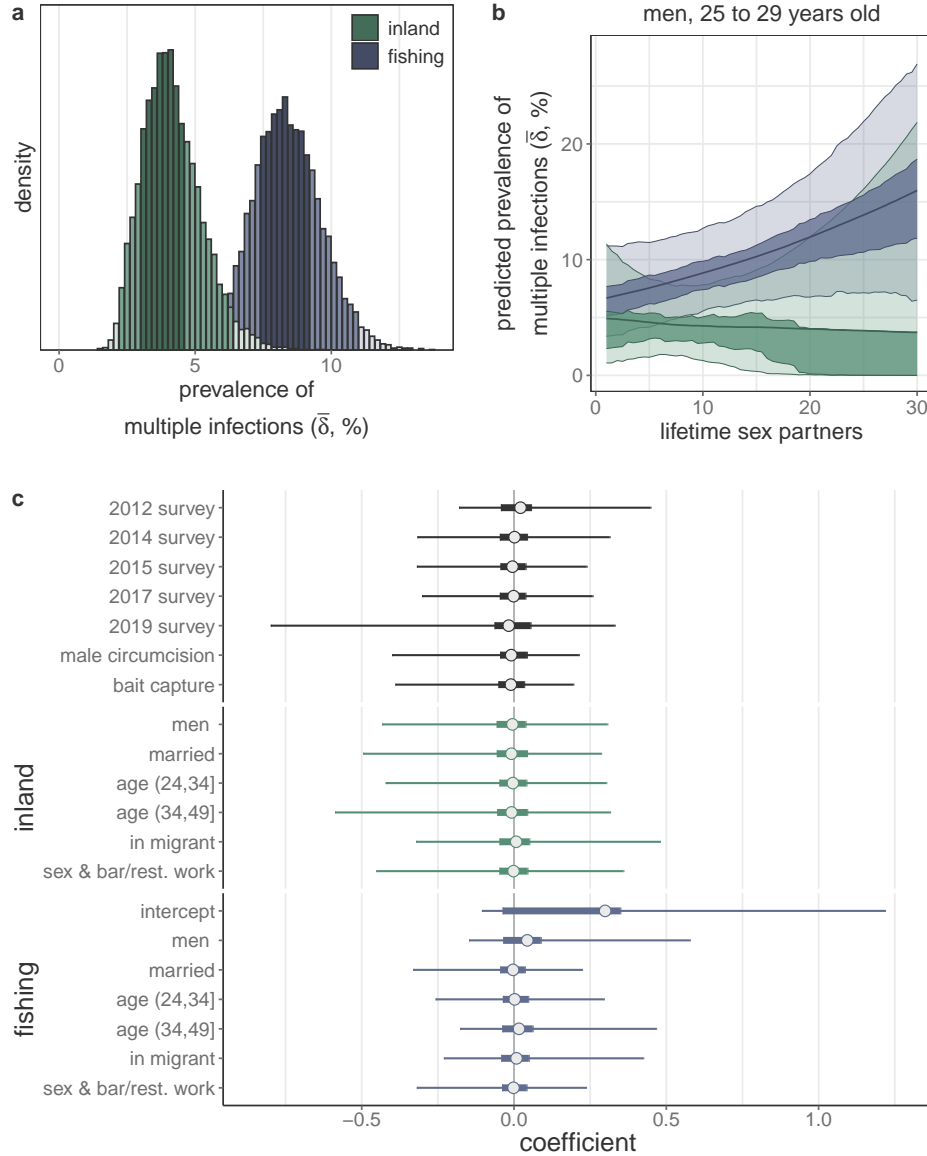


Fig 4. Risk factors of HIV multiple infection among people with viremic HIV in the Rakai Community cohort Study, 2010-2020. (A) Posterior distribution of the prevalence of multiple infections stratified by community type estimated in a univariate model with diffuse priors ($N = 2,029$). Bins are shaded according to the 95% and 50% highest posterior density (HPD). Histogram width is calculated such that there are approximately 50 bins over the range of plotted values. (B) Predicted prevalence of multiple infection among men aged 25 to 29 years old as a function of lifetime sex partners and community type estimated in a bivariate model with diffuse priors ($N = 997$). Median of the posterior distribution is plotted as the central estimate and shading represents the 95% and 50% HPD. Colors are as in (A). (C) Logistic coefficients for the association between putative risk factors and the probability of harboring a multiple infection estimated with Bayesian shrinkage priors ($N = 1,970$). Sex and bar/rest. work variable includes female sex and bar/restaurant worker and men who report having sex with female sex and bar/restaurant workers. Median of the posterior distribution is plotted as the central estimate, horizontal bars extend to the 95% and 50% HPD. Colors are as in (A).

could potentially be due to recombination between infecting lineages prior to sampling [5,6] such that infecting variants are only genetically distinct in some portions of genome when sampled. The population-based

436
437

multiple infection prevalence estimates from the data reported here are substantially more precise than previous estimates from this setting as expected given the larger sample size and slightly higher than previous estimates ($n = 7/149$ [3]), likely reflecting greater sensitivity of whole-genome sequencing data. Previous studies of female sex workers in urban Uganda and Kenya have estimated the prevalence of multiple infections to be as high as 14 – 16% in this high-risk demographic based on amplicon deep-sequencing [30,31]. Here, we do not replicate this finding using self-reported data on sex work or bar/restaurant work in our population-based sampling framework. We expect this is likely due to hesitation to self-report sex work among study participants and study participation bias among sex workers. However, our results are generally consistent with previous findings suggesting MIs are less common in African populations as compared to the United States (10-15% in studies conducted between 1996 and 2010 [91–95]), which may reflect the fact that the HIV epidemic in the United States is concentrated among men who have sex with men (MSM) and people who inject drugs (PWID) as opposed to the generalized nature of the epidemic in Africa. Further, as the risk of HIV transmission given exposure is 8-16 \times and 3-17 \times greater for needle-sharing and anal intercourse, respectively, as compared to vaginal intercourse [96], the risk of multiple infection acquisition given exposure may also be significantly greater in concentrated epidemics. To date, however, we note that the sample size of HIV multiple infection studies in the United States are relatively small (<150 individuals) and there is therefore significant uncertainty in the true underlying prevalence in these settings.

Our results add to the considerable previous research on the increased risk of HIV among Lake Victoria fishing communities. Previous studies have shown that overall HIV prevalence and prevalence of viremic HIV in these communities is 2.5-3 \times higher than in inland communities [36,89], in part due to migration of PLHIV to these communities [97,98]. Further, despite a rapid increase in antiretroviral therapy (ART) uptake among residents of fishing communities over the study period [99], there remains a higher prevalence of people living with viremic, ART-resistant HIV as compared to inland communities [100]. We here show that viremic PLHIV in fishing communities also face a significantly higher burden of HIV multiple infections. We also show that among men in fishing communities, multiple infection risk increases with the number of lifetime sex partners. The precision of this estimate is hindered by a large degree of non-precise responses to this component of the RCCS survey. These results imply that PLHIV in fishing communities continue to be exposed to viremic partners following initial infection. Public health interventions directed at viremic PLHIV in these communities may therefore not only provide life-saving treatment to these individuals but also reduce opportunities for the generation of novel recombinant forms of HIV which could pose challenges to control efforts through potential generation of more transmissible variants and broadening the antigenic space that potential vaccines need to cover [5,6,10–12,101].

We expect that our inferential framework may be adaptable to whole-genome deep-sequence phylogenies from other pathogens in which infection is chronic (thereby allowing sufficient time for superinfection to occur). Hepatitis C virus (HCV), which is a chronic viral infection transmitted either sexually or by injection drug use, is a natural extension [102]. Among people who inject drugs, the prevalence of HCV mixed infections is estimated to be as high as 39% [103]. Our framework has the advantage that it uses data from across the genome and does not require haplotyping of sequencing reads, which has proven to be exceedingly difficult with short-read sequence data [104]. Recent work has also attempted to identify multiple infections of *Mycobacterium tuberculosis* (MTB), a chronic bacterial infection canonically of the lungs [105]. These methods work by either clustering allele frequencies to distinguish within- and between-variant differences [106–108] or by comparing sampled sequence data to a database of reference strains [109]. They therefore require defining circulating genetic diversity *a priori* (which may be challenging in a poorly sampled epidemic) or assume independence between alleles, failing to account for linkage between adjacent genome positions and the evolutionary history giving rise to the observed genetic variation. Multiple infections may also be of interest in acute, high-prevalence infectious diseases. For example, severe acute respiratory syndrome coronavirus 2 (SARS-CoV-2) superinfections have been observed by identifying mixed alleles as known lineage-defining sites [110,111].

While *deep-phyloMI* builds upon previous investigations into HIV multiple infections to provide more rigorous estimates of individual and population level parameters, we do rely on some simplifying assumptions in our framework. First, we only identify multiple infections among viremic participants with available deep-sequence data who were identified as part of a putative transmission network. This sample may therefore be non-representative of the underlying population of viremic PLHIV. Because the RCCS did not perform viral load testing on all participants prior to the 2014 survey round we lack the necessary

data to reliably account for these biases in a weighted analysis. Further, we focus on identifying multiple infections only in cross-sectional sequence data. As multiple infections can be transient [31], we are unable to identify participants who have been but are not currently multiply infected. Similarly, in the absence of longitudinal data or data sampled soon after initial infection we are unable to distinguish multiple infections acquired through coinfection and superinfection. Further, our inferences are likely sensitive to settings within *phyloscanner*. Specifically, clustering of within-host phylogenetic subgraphs is dependent on the k parameter used in the ancestral state reconstruction. While our model is tolerant of some misspecification of k due to the modeled false-positive and false-negative rates, participants infected with multiple genetically distinct yet similar variants may remain undetected given the conservative k value we employed based on the circulating genetic diversity in our study setting [9]. We therefore expect our estimates to represent a lower bound of the true prevalence among sequenced participants. More liberal values of k would increase the sensitivity of this approach, potentially suitable to settings with less circulating genetic diversity, at the expense of specificity.

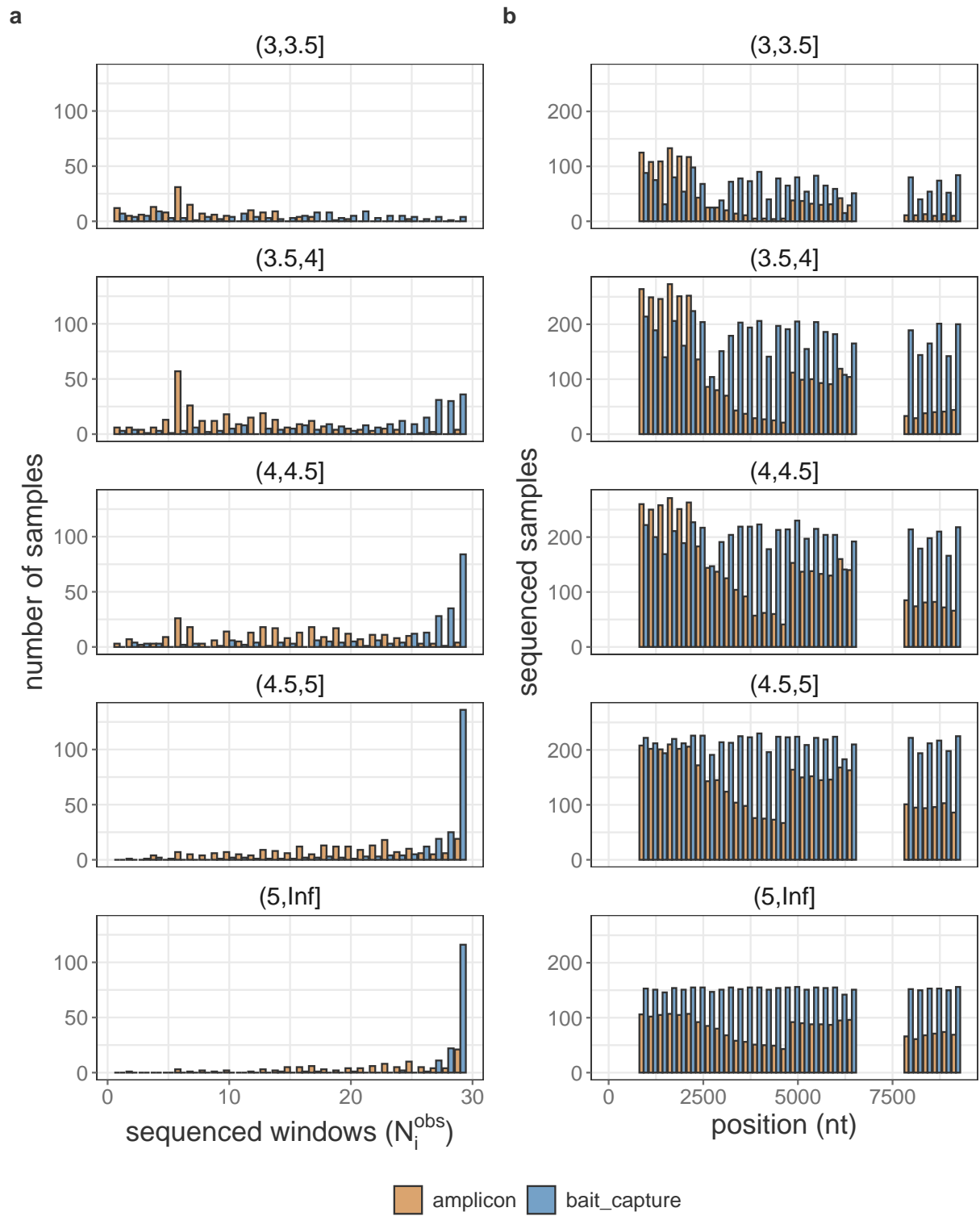
HIV multiple infections complicate global control efforts by fueling generation of genetic diversity [8], worsening clinical outcomes [13,14], and increasing viral load [14,16,31]. Here we developed a robust inference framework to identify multiple infections in deep-sequence data and assess the role of epidemiological risk factors, such as living in high burden communities, in harboring multiple infections. This work will inform interventions aimed at preventing the acquisition of HIV superinfections and efforts to model the role of multiple infections in the dynamics and evolution of HIV.

Acknowledgments

We thank the participants of the Rakai Community Cohort Study for making this research possible. Further, we thank all Rakai Health Sciences Program staff and all members of the PANGAEA-HIV consortium. We thank Dr. Chris Wymant, PhD (Pandemic Sciences Institute, University of Oxford) for helpful discussions about Bayesian modeling of HIV multiple infections and helpful comments on this manuscript. Computational resources were provided through the Imperial College Research Computing Service and the Biomedical Research Computing Cluster at the University of Oxford. This study was supported by the Bill and Melinda Gates Foundation (OPP1084362, INV-007573, INV-035619, INV-060259, INV-075093), the National Institute of Health (NIH) National Institute of Allergy and Infectious Diseases (NIAID, U01AI075115, R01AI087409, U01AI100031, R01AI110324, R01AI114438, K25AI114461, R01AI123002, K01AI125086, R01AI128779, R01AI143333, R21AI145682, R01AI155080, ZIAAI001040), NIH National Institute of Child Health and Development (R01HD050180, R01HD070769, R01HD091003), NIH National Heart, Lung, and Blood Institute (R01HL152813), the Fogarty International Center (D43TW009578, D43TW010557), the Johns Hopkins University Center for AIDS Research (P30AI094189), the U.S. President’s Emergency Plan for AIDS Relief through the Centers for Disease Control and Prevention (NU2GGH000817), and in part by the Division of Intramural Research, NIAID, NIH. MM was supported in part by NIH 1L30AI178824.

Supporting information

526



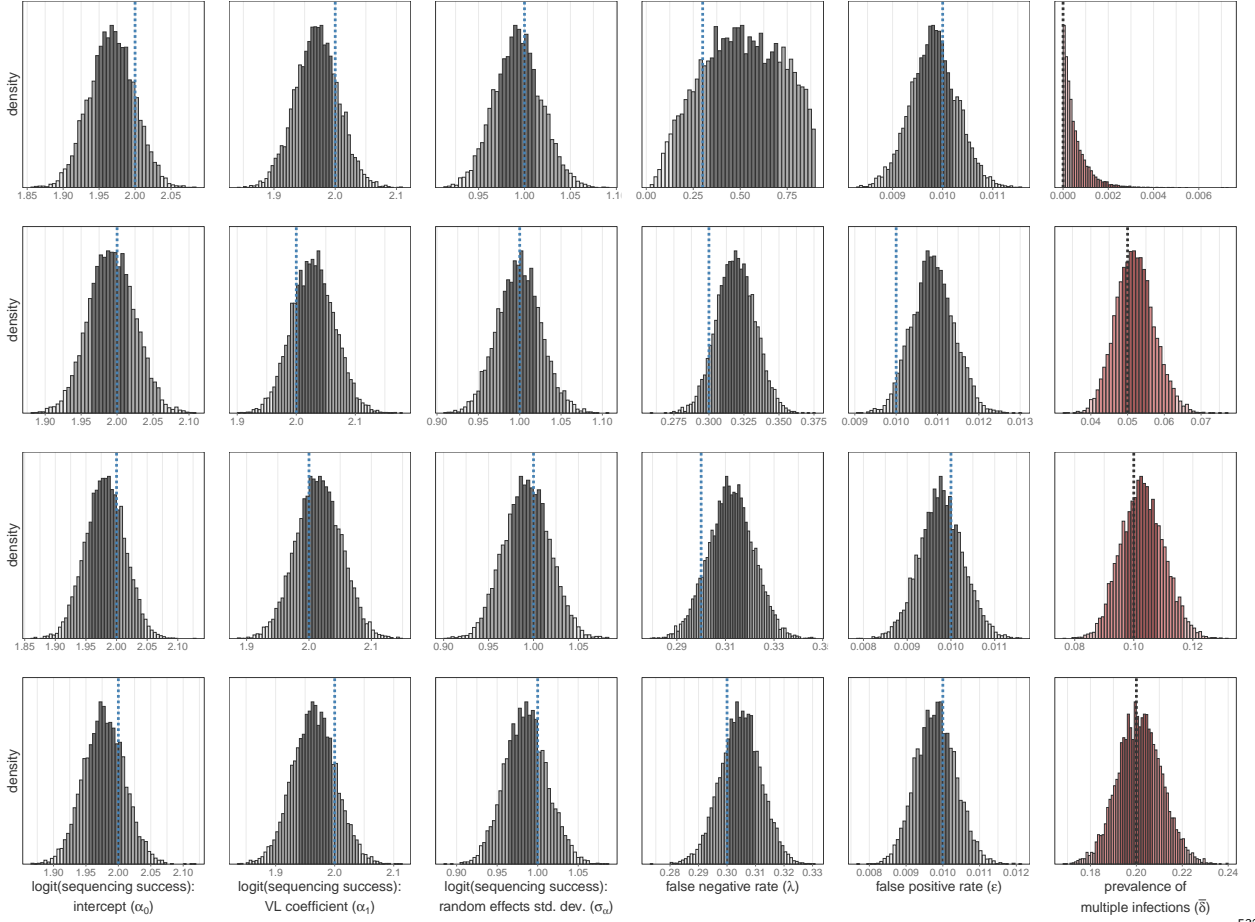
527

S1 Fig. Sequencing coverage among samples from 2,029 Rakai Community Cohort Study participant-visits contributed by viremic people living with HIV with $N_i^{obs} > 0$, stratified by

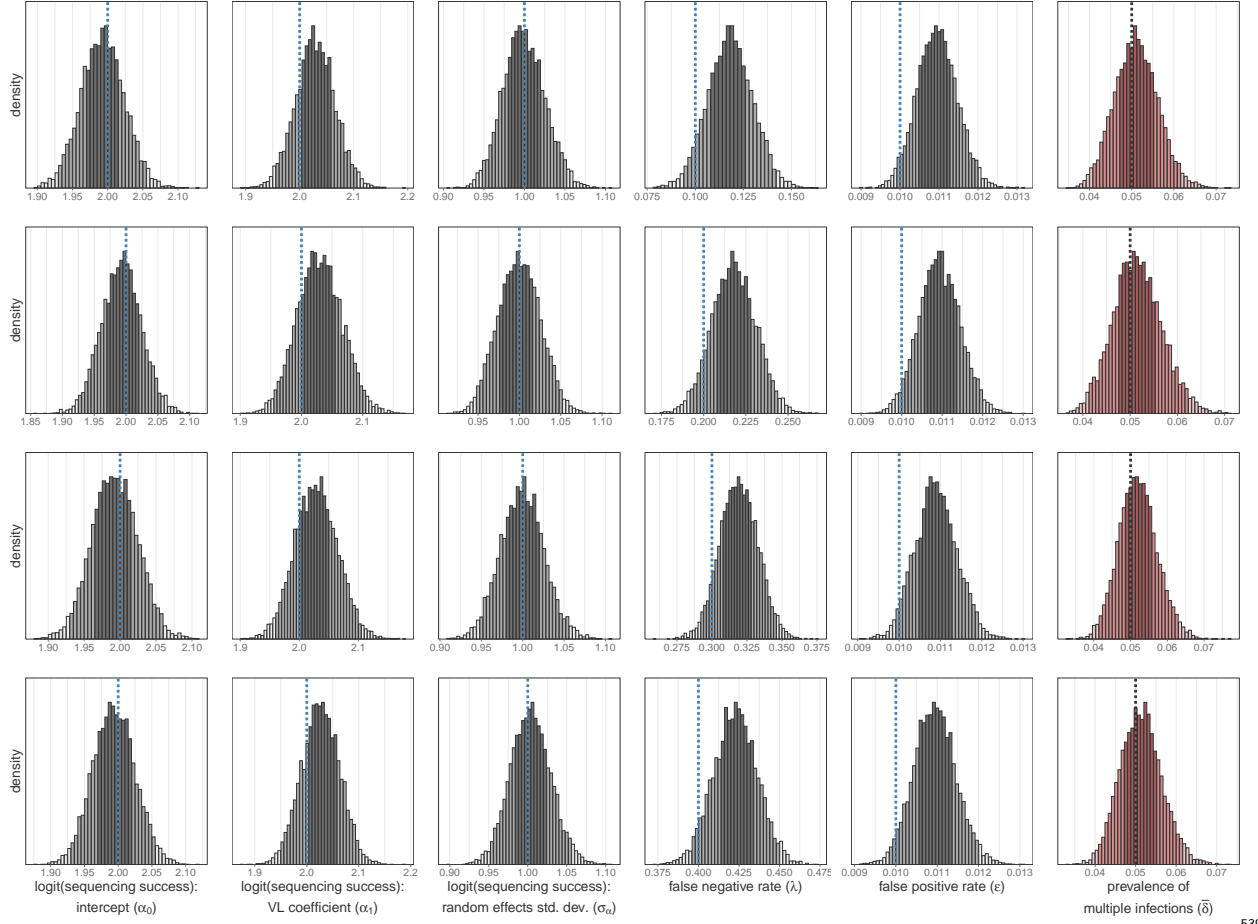
528

529

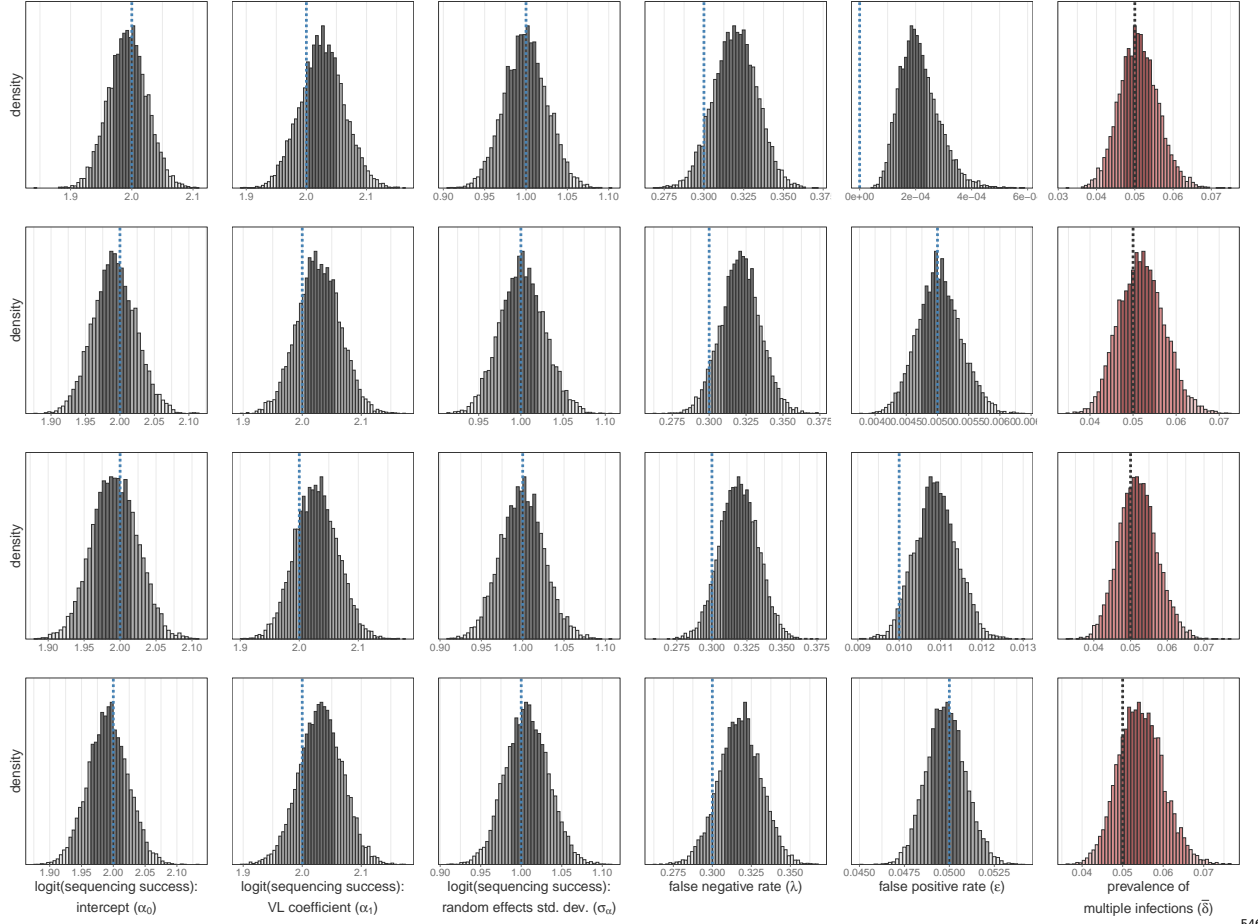
viral load category and sequencing technology. (A) Distribution of N_i^{obs} values for all samples. (B) Number of samples with coverage in each of the 29 genome window. 530
531



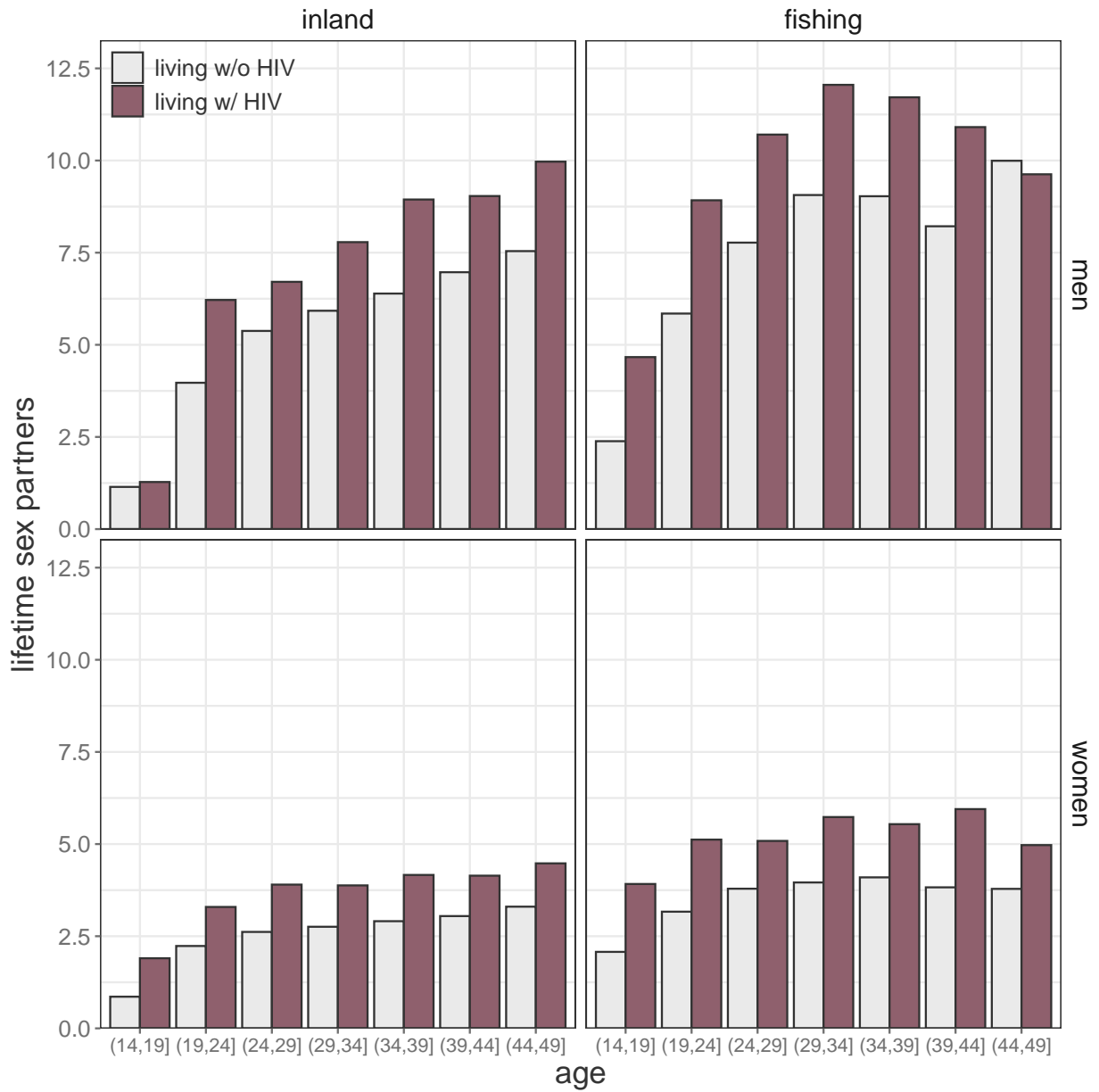
S2 Fig. Posterior distribution of parameters in full model fit to simulated data across a range of δ values. Rows represent model to fit to simulated data with $\delta = 0$ (top row), $\delta = 5\%$ (second row), $\delta = 10\%$ (third row), and $\delta = 20\%$ (bottom row). Posterior distributions bins are shaded according to the 95% and 50% highest posterior density. Histogram width is calculated such that there are approximately 50 bins over the range of plotted values. True values are shown as vertical dotted lines. VL = viral load (\log_{10} copies/mL) normalized to mean = 0 and std. dev = 1. Std. dev. = standard deviation. 533
534
535
536
537
538



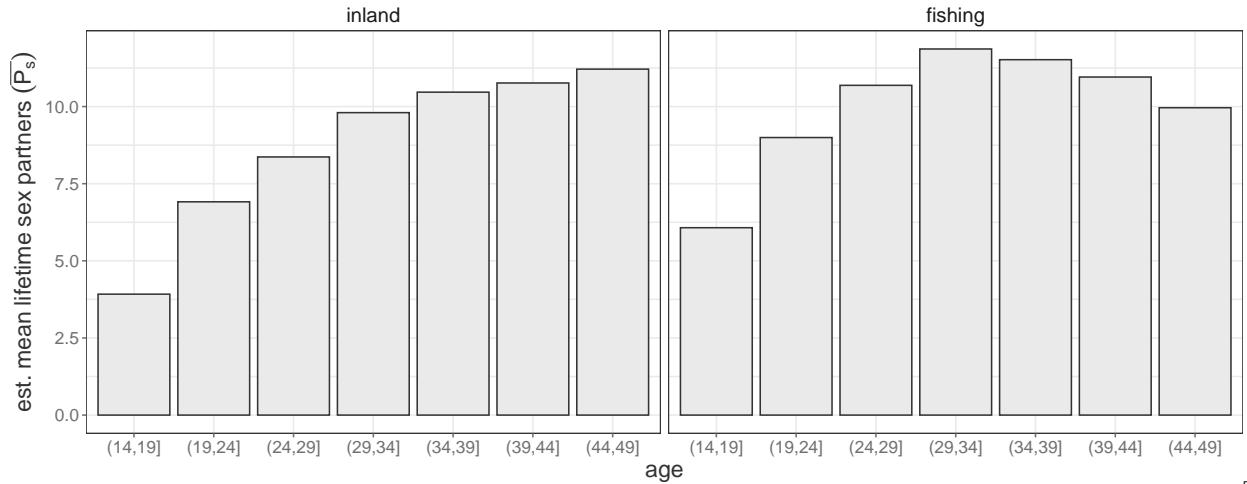
S3 Fig. Posterior distribution of parameters in full model fit to simulated data across a range of λ values. Rows represent model to fit to simulated data with $\lambda = 0.1$ (top row), $\lambda = 0.2\%$ (second row), $\lambda = 0.3\%$ (third row), and $\lambda = 0.4\%$ (bottom row). Posterior distributions bins are shaded according to the 95% and 50% highest posterior density. Histogram bin width is calculated such that there are approximately 50 bins over the range of the plotted values. True values are shown as vertical dotted lines. VL = viral load (\log_{10} copies/mL) normalized to mean = 0 and std. dev = 1. Std. dev. = standard deviation.



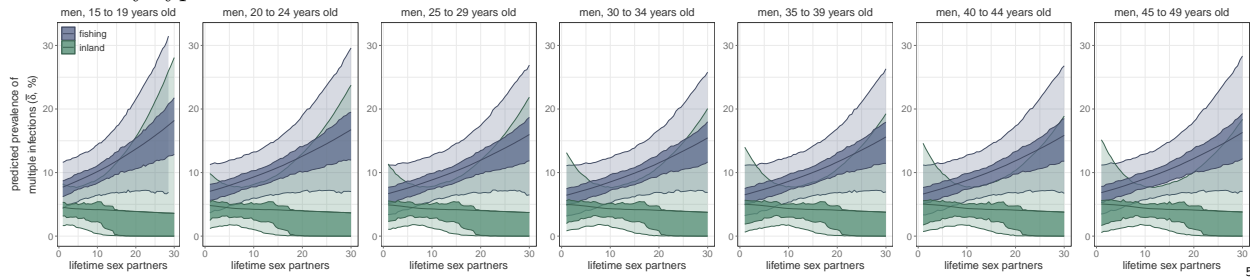
S4 Fig. Posterior distribution of parameters in full model fit to simulated data across a range of ϵ values. Rows represent model to fit to simulated data with $\epsilon = 0$ (top row), $\epsilon = 0.5\%$ (second row), $\epsilon = 1\%$ (third row), and $\epsilon = 5\%$ (bottom row). Posterior distributions bins are shaded according to the 95% and 50% highest posterior density. Histogram bin width is calculated such that there are approximately 50 bins over the range of the plotted values. True values are shown as vertical dotted lines. VL = viral load (\log_{10} copies/mL) normalized to mean = 0 and std. dev = 1. Std. dev. = standard deviation.



S5 Fig. Mean number of lifetime sex partners stratified by HIV serostatus, sex, community type, and age among 109,608 RCCS participant-visits. Excludes participant visits in which respondents provided a categorical response (N=5,436 (10.67%)).



S6 Fig. Standardization curve used to adjust observed number of lifetime sex partners among men for age-cohort effects. Includes simple imputation of categorical responses (e.g. “1-2” and “3+”) to 1) the mean value of observed responses of 1 or 2 (“1-2”) within age category and community type and 2) the mean of a lognormal distribution fit to observed responses of ≥ 3 lifetime sex partners within age category and community type.



S7 Fig. Posterior estimates of the prevalence of multiple infections, stratified by age category and community type. Median estimate is plotted as a line and shading represents the 50% and 95% highest posterior densities. All age categories share the same coefficient estimates but differ because lifetime sex partner values are standardized to the mean of the observed values within groups defined by sex, age category, and community type.

S1 File.	Supplementary methods.	569
S2 File.	Reference genomes included in the <i>phyloscanner</i> analysis.	570
S3 File.	Normalization constants used to adjust branch lengths in within-host phylogenetic trees.	571 572
S4 File.	Bayesian model fit diagnostics.	573
S5 File.	Sensitivity of results to choice of non-overlapping genome windows.	574

S1 Table.

Survey round	Participants	
	amplicon (PANGA1)	bait-capture (PANGA2)
2010	0	16
2012	720	29
2014	296	50
2015	14	509
2017	0	328
2019	0	67

Count of participants sequenced using each sequencing protocol.

575

S2 Table.

	All	Participants Living w/ HIV (%)	
		<i>n</i> (%)	% of All
Overall	50,967	8,841	19,503
Survey Round			
2010	15,663 (30.73%)	1,812 (21.72%)	11.57% (11.08% - 12.08%)
2012	9,985 (19.59%)	2,202 (26.4%)	22.05% (21.25% - 22.88%)
2014	7,032 (13.8%)	1,170 (14.03%)	16.64% (15.79% - 17.53%)
2015	6,364 (12.49%)	1,292 (15.49%)	20.3% (19.33% - 21.31%)
2017	6,158 (12.08%)	1,080 (12.95%)	17.54% (16.61% - 18.51%)
2019	5,765 (11.31%)	786 (9.42%)	13.63% (12.77% - 14.54%)
Sex			
Female	27,621 (54.19%)	5,315 (63.71%)	19.24% (18.78% - 19.71%)
Male	23,346 (45.81%)	3,027 (36.29%)	12.97% (12.54% - 13.4%)
Community type			
Inland	41,508 (81.44%)	4,974 (59.63%)	11.98% (11.67% - 12.3%)
Fishing	9,459 (18.56%)	3,368 (40.37%)	35.61% (34.65% - 36.58%)
Age			
(14, 24]	24,356 (47.79%)	1,472 (17.65%)	6.04% (5.75% - 6.35%)
(24, 34]	24,356 (31.38%)	3,875 (46.45%)	24.23% (23.57% - 24.9%)
(34, 49]	10,616 (20.83%)	2,995 (35.9%)	28.21% (27.36% - 29.08%)

Characteristics of Rakai Community Cohort Study participant, 2010-2020. For each participant, includes data from the participant-visit processed with PHSC if applicable or the participant-visit with the highest viral load, using the first visit in the case of ties or for people not living with HIV. Percentages represent the row percentages within each category. Binomial confidence intervals were calculated using the Agresti–Coull method. PHSC = phyloscanner.

576

S3 Table.

Variable	Participant-visits with missing data (%)	
	All (%)	Viremic & Processed w PHSC (%)
HIV serostatus	104 (0.2%)	0 (0%)
Sex	0 (0%)	0 (0%)
Age	0 (0%)	0 (0%)
Circumcision	5791 (11.36%)	54 (2.66%)
Community type	0 (0%)	0 (0%)
Married	7 (0.01%)	0 (0%)
Lifetime sex partners	0 (0%)	0 (0%)
In-migrant	179 (0.35%)	5 (0.25%)
Sex & bar/restaurant work	27 (0.05%)	0 (0%)

Count of missing values among 50,967 RCCS participants. For each participant, includes data from the participant-visit processed with PHSC if applicable or the participant-visit with the highest viral load, using the first visit in the case of ties or for people not living with HIV. In each category the percentage represents the percentage of all participants or all participants that were viremic and processed with PHSC.

577

S4 Table.

Parameter	True Value	Prior	Median (95% HPD)	Bulk ESS	Tail ESS	\hat{R}
α_0	2	Normal(0,2 ²)	1.99 (1.93, 2.05)	2185.95	3748.22	1
α_1	2	Normal(0,2 ²)	2.02 (1.95, 2.1)	2506.19	3379.78	1
σ_α	1	Half-Cauchy(0,1)	1 (0.95, 1.05)	2619.47	5233.23	1
δ_0	-2.94	Normal(0,3.16 ²)	-2.92 (-3.13, -2.72)	8235.07	4912.29	1

Parameter estimates for base model fit to base simulated data. ESS = effective sample size. HPD = highest posterior density.

578

S5 Table.

Parameter	True Value	Prior	Median (95% HPD)	Bulk ESS	Tail ESS	\hat{R}
α_0	2	Normal(0,2 ²)	1.2 (1.13, 1.28)	1236.21	2393.59	1
α_1	2	Normal(0,2 ²)	1.39 (1.3, 1.46)	1321.8	2523.37	1
σ_α	1	Half-Cauchy(0,1)	1.51 (1.44, 1.57)	4696.51	6324.78	1
δ_0	-2.94	Normal(0,3.16 ²)	-1.02 (-1.12, -0.91)	17682.32	5782.47	1

Parameter estimates for base model fit to full simulated data. ESS = effective sample size. HPD = highest posterior density.

579

S6 Table.

Parameter	True Value	Prior	Median (95% HPD)	Bulk ESS	Tail ESS	\hat{R}
α_0	2	Normal(0,2 ²)	1.99 (1.93, 2.06)	2646.13	3927.62	1
α_1	2	Normal(0,2 ²)	2.03 (1.96, 2.1)	2475.9	4405.79	1
σ_α	1	Half-Cauchy(0,1)	1 (0.95, 1.05)	2427.35	3585.93	1
δ_0	-2.94	Normal(0,3.16 ²)	-2.91 (-3.12, -2.7)	11718.68	5800.08	1
logit(λ)	-0.85	Normal(0,1)	-0.76 (-0.89, -0.64)	9051.87	5946.11	1
logit(ϵ)	-4.6	Normal(0,1)	-4.51 (-4.6, -4.42)	11908.52	5061.41	1

Parameter estimates for full model fit to full simulated data. ESS = effective sample size. HPD = highest posterior density.

580

S7 Table.

Parameter	True Value	Prior	Median (95% HPD)	Bulk ESS	Tail ESS	\hat{R}
α_0	2	Normal(0,2 ²)	2 (1.94, 2.06)	2536.89	4489.11	1
α_1	2	Normal(0,2 ²)	1.99 (1.92, 2.07)	2744.28	4770.11	1
σ_α	1	Half-Cauchy(0,1)	0.99 (0.94, 1.04)	3008.67	4623.96	1
δ_0	-2.94	Normal(0,3.16 ²)	-2.79 (-3.2, -2.4)	6767.17	5712.9	1
logit(λ)	-0.85	Normal(0,1)	-0.72 (-0.81, -0.62)	13012.54	6450.52	1
logit(ϵ)	-4.6	Normal(0,1)	-4.55 (-4.65, -4.46)	12175.43	5227.47	1
β_1	0.75	Normal(0, $\xi_1^2\tau^2$)	0.6 (0.17, 1.03)	4892.8	3210.09	1
β_2	0	Normal(0, $\xi_2^2\tau^2$)	0 (-0.25, 0.26)	9734.48	7714.16	1
β_3	0	Normal(0, $\xi_3^2\tau^2$)	-0.07 (-0.44, 0.14)	5858.23	7024.1	1
β_4	0	Normal(0, $\xi_4^2\tau^2$)	0 (-0.27, 0.23)	10058.67	7566.46	1
β_5	0	Normal(0, $\xi_5^2\tau^2$)	-0.03 (-0.34, 0.18)	8377.08	7284.92	1
τ	0	Half-Cauchy(0,1)	-0.03 (-0.34, 0.18)	8377.08	7284.92	1
ξ_1	-	Half- $t_2(0, 1)$	1.73 (0.02, 7.27)	6259.68	4166.5	1
ξ_2	-	Half- $t_2(0, 1)$	0.47 (0, 2.22)	5718.96	4258.51	1
ξ_3	-	Half- $t_2(0, 1)$	0.6 (0, 2.64)	4189.42	3208.36	1
ξ_4	-	Half- $t_2(0, 1)$	0.49 (0, 2.18)	6455.44	5090.41	1
ξ_5	-	Half- $t_2(0, 1)$	0.51 (0, 2.37)	5450.67	4335.94	1

Parameter estimates for extended model fit to extended simulated data with epidemiological risk factor of multiple infection. ESS = effective sample size. HPD = highest posterior density.

581

S8 Table.

Parameter	Prior	Median (95% HPD)	Bulk ESS	Tail ESS	\hat{R}
α_0	Normal(0,2 ²)	-0.08 (-0.18, 0.01)	1094.34	2116.52	1
α^{bait}	Normal(0,2 ²)	2.61 (2.45, 2.76)	1522.61	3106.93	1
$\alpha^{amplicon-vl}$	Normal(0,2 ²)	0.85 (0.76, 0.95)	1513.14	2991.73	1
$\alpha^{bait-vl}$	Normal(0,2 ²)	1.52 (1.38, 1.63)	2283.44	3711.07	1
σ_α	Half-Cauchy(0,1)	1.52 (1.45, 1.59)	4631.32	6140	1
δ_0	Normal(0,3.16 ²)	-2.79 (-3.03, -2.56)	7236.45	4682.27	1
logit(λ)	Normal(0,1)	0.29 (0.12, 0.47)	5004.3	5833.33	1
logit(ϵ)	Normal(0,1)	-5.73 (-5.96, -5.5)	4917.44	5128.91	1

Parameter estimates for full model fit to deep-sequence data from 2,029 RCCS participants living with viremic HIV. ESS = effective sample size. HPD = highest posterior density.

582

S9 Table.

Parameter	Prior	Median (95% HPD)	Bulk ESS	Tail ESS	\hat{R}
α_0	Normal(0,2 ²)	-0.09 (-0.19, 0.01)	1146.2	1814.41	1
α^{bait}	Normal(0,2 ²)	2.61 (2.46, 2.78)	1169.91	2091.67	1
$\alpha^{amplicon-vl}$	Normal(0,2 ²)	0.86 (0.76, 0.95)	1305.16	2202.41	1
$\alpha^{bait-vl}$	Normal(0,2 ²)	1.51 (1.38, 1.64)	2171.41	3907.97	1
σ_α	Half-Cauchy(0,1)	1.52 (1.46, 1.59)	4013.69	5383.67	1
δ_0	Normal(0,3.16 ²)	-3.16 (-3.73, -2.67)	5543.81	5487.07	1
β_1 (fishing)	Normal(0,1)	0.76 (0.27, 1.3)	7418.81	6411.46	1
β_2 (bait)	Normal(0,1)	-0.28 (-0.7, 0.17)	7430	5696.73	1
logit(λ)	Normal(0,1)	0.31 (0.13, 0.49)	4610.3	6765.86	1
logit(ϵ)	Normal(0,1)	-5.75 (-5.99, -5.52)	4828.24	5368.65	1

Parameter estimates for full model fit to deep-sequence data from 2,029 RCCS participants living with viremic HIV with community type as a putative risk factor for harboring multiple infections ESS = effective sample size. HPD = highest posterior density.

583

S10 Table.

Parameter	Prior	Median (95% HPD)	Bulk ESS	Tail ESS	\hat{R}
α_0	Normal(0,2 ²)	-0.09 (-0.19, 0)	525.87	1229.28	1
α^{bait}	Normal(0,2 ²)	2.61 (2.46, 2.78)	657.52	1460.72	1
$\alpha^{amplicon-vl}$	Normal(0,2 ²)	0.86 (0.76, 0.95)	646.06	1269.78	1
$\alpha^{bait-vl}$	Normal(0,2 ²)	1.52 (1.39, 1.64)	942.2	1762.16	1
σ_α	Half-Cauchy(0,1)	1.52 (1.45, 1.59)	2843.24	4276.61	1
δ_0	Normal(0,3.16 ²)	-2.54 (-2.86, -2.25)	3234	5148.56	1
β_1 (bait)	Normal(0,1)	-0.45 (-0.87, -0.03)	3981.07	5737	1
logit(λ)	Normal(0,1)	0.29 (0.11, 0.46)	2888.58	4248.63	1
logit(ϵ)	Normal(0,1)	-5.73 (-5.96, -5.5)	3106.38	4689.05	1

Parameter estimates for full model fit to deep-sequence data from 2,029 RCCS participants living with viremic HIV with deep-sequencing protocol as a predictor harboring multiple infections. ESS = effective sample size. HPD = highest posterior density.

S11 Table.

Parameter	Prior	Median (95% HPD)	Bulk ESS	Tail ESS	\hat{R}
α_0	Normal(0,2 ²)	0.03 (-0.13, 0.19)	1339.58	2427.25	1
α^{bait}	Normal(0,2 ²)	2.78 (2.55, 3.02)	1753.89	3032.01	1
$\alpha^{amplicon-vl}$	Normal(0,2 ²)	0.87 (0.72, 1.03)	1543.34	2738.45	1
$\alpha^{bait-vl}$	Normal(0,2 ²)	1.45 (1.27, 1.63)	2386.46	4352.04	1
σ_α	Half-Cauchy(0,1)	1.57 (1.47, 1.67)	3828.27	5678.22	1
δ_0	Normal(0,3.16 ²)	-3.1 (-3.93, -2.39)	6078.09	5053.03	1
β_1 (fishing)	Normal(0,1)	0.78 (0.11, 1.55)	7428.5	5205.68	1
β_2 (bait)	Normal(0,1)	-0.17 (-0.72, 0.38)	9545.07	6134.2	1
β_3 (inland:sexpever)	Normal(0,1)	-0.01 (-0.17, 0.1)	4917.47	5644.04	1
β_4 (fishing:sexpever)	Normal(0,1)	0.03 (0, 0.07)	4686.68	5224.49	1
logit(λ)	Normal(0,1)	0.51 (0.32, 0.69)	7346.01	5940.72	1
logit(ϵ)	Normal(0,1)	-5.92 (-6.25, -5.6)	6534.59	6058.7	1

Parameter estimates for full model fit to deep-sequence data from 997 men who participated in the RCCS living with viremic HIV with community type and number of lifetime sex partners as a risk factor for harboring multiple infections adjusted for deep-sequencing protocol.. ESS = effective sample size. HPD = highest posterior density.

585

S12 Table.

Parameter	Prior	Median (95% HPD)	Bulk ESS	Tail ESS	\hat{R}
α_0	Normal(0,2 ²)	0.11 (-0.07, 0.31)	716.17	1357.05	1
α^{bait}	Normal(0,2 ²)	2.38 (2.08, 2.7)	820.82	1636.68	1
$\alpha^{amplicon-vl}$	Normal(0,2 ²)	0.93 (0.74, 1.11)	796.43	1657.19	1.01
$\alpha^{bait-vl}$	Normal(0,2 ²)	1.2 (0.95, 1.45)	1066.29	2056.84	1
σ_α	Half-Cauchy(0,1)	1.51 (1.38, 1.64)	2916.56	5210.72	1
δ_0	-3.22 (-4.25, -2.21)	2833.64	3766.81	1	
β_1 (fishing)	Normal(0,1)	1.09 (0.15, 2.1)	3272.91	4008.3	1
β_2 (bait)	Normal(0,1)	-0.37 (-1.19, 0.41)	6469.05	5471.96	1
β_3 (inland:sexpever)	Normal(0,1)	-0.02 (-0.19, 0.1)	5411.12	4042.59	1
β_4 (fishing:sexpever)	Normal(0,1)	0.03 (0, 0.07)	4007.77	4906.82	1
logit(λ)	Normal(0,1)	0.73 (0.41, 1.04)	3562.87	5578.15	1
logit(ϵ)	Normal(0,1)	-5.84 (-6.34, -5.37)	3775.04	5281.16	1

Parameter estimates for full model fit to deep-sequence data from 516 men who participated in the RCCS living with viremic HIV with community type and number of lifetime sex partners as a risk factor for harboring multiple infections. Excludes participants with ambiguous or missing data on the number of lifetime sex partners. ESS = effective sample size. HPD = highest posterior density.

586

S13 Table.

587

Parameter	Prior	Median (95% HPD)	Bulk ESS	Tail ESS	\hat{R}
α_0	Normal(0,2 ²)	-0.09 (-0.19, 0.02)	837.75	1484.8	1
α^{bait}	Normal(0,2 ²)	2.63 (2.47, 2.79)	864.33	1965.51	1
$\alpha^{amplicon-vl}$	Normal(0,2 ²)	0.87 (0.77, 0.97)	921.69	2317.86	1
$\alpha^{bait-vl}$	Normal(0,2 ²)	1.52 (1.39, 1.65)	1126.56	2436.46	1
σ_α	Half-Cauchy(0,1)	1.53 (1.47, 1.6)	3666.66	5360.88	1
δ_0	Normal(0, 3.16 ²)	-3.08 (-3.85, -2.54)	2837.74	3621.39	1
β_1 (2012 survey)	Normal(0, $\xi^2 \tau^2$)	0.02 (-0.18, 0.45)	7245.51	7140.83	1
β_2 (2014 survey)	Normal(0, $\xi^2 \tau^2$)	0 (-0.32, 0.31)	5964.5	1549.83	1
β_3 (2015 survey)	Normal(0, $\xi^2 \tau^2$)	-0.01 (-0.32, 0.24)	8421.54	6564.58	1
β_4 (2017 survey)	Normal(0, $\xi^2 \tau^2$)	0 (-0.3, 0.26)	8990.45	7144.04	1
β_5 (2019 survey)	Normal(0, $\xi^2 \tau^2$)	-0.02 (-0.8, 0.33)	5241.28	5275.69	1
β_6 (male circumcision)	Normal(0, $\xi^2 \tau^2$)	-0.01 (-0.4, 0.21)	8738.47	7427.83	1
β_7 (fishing)	Normal(0, $\xi^2 \tau^2$)	0.3 (-0.11, 1.22)	2090.19	4116.45	1
β_8 (bait)	Normal(0, $\xi^2 \tau^2$)	-0.01 (-0.39, 0.2)	8077.58	6284.62	1
β_9 (inland: male)	Normal(0, $\xi^2 \tau^2$)	-0.01 (-0.43, 0.31)	7324.33	6642.86	1
β_{10} (fishing: male)	Normal(0, $\xi^2 \tau^2$)	0.04 (-0.15, 0.58)	3314.58	1522.5	1
β_{11} (inland: married)	Normal(0, $\xi^2 \tau^2$)	-0.01 (-0.5, 0.29)	7415.64	5418.41	1
β_{12} (fishing: married)	Normal(0, $\xi^2 \tau^2$)	0 (-0.33, 0.22)	7880.17	7198.54	1
β_{13} (inland: (24,34 years])	Normal(0, $\xi^2 \tau^2$)	0 (-0.42, 0.3)	7488.31	4936.84	1
β_{14} (Fishing: (24,34 years])	Normal(0, $\xi^2 \tau^2$)	0 (-0.26, 0.3)	9362.47	7388.62	1
β_{15} (inland: (34,49] years])	Normal(0, $\xi^2 \tau^2$)	-0.01 (-0.59, 0.32)	4871.52	1575.23	1
β_{16} (fishing: (34,49] years])	Normal(0, $\xi^2 \tau^2$)	0.02 (-0.18, 0.47)	7563.45	7515.7	1
β_{17} (inland: in migrant)	Normal(0, $\xi^2 \tau^2$)	0.01 (-0.32, 0.48)	5595.16	4250.7	1
β_{18} (fishing: in migrant)	Normal(0, $\xi^2 \tau^2$)	0.01 (-0.23, 0.42)	8559.46	6865.78	1
β_{19} (inland: sex & bar/rest. worker)	Normal(0, $\xi^2 \tau^2$)	0 (-0.45, 0.36)	8079.66	6377.58	1
β_{20} (fishing: sex & bar/rest. worker)	Normal(0, $\xi^2 \tau^2$)	0 (-0.32, 0.24)	5655.2	1593.87	1
τ	Half-Cauchy(0, 1)	0.13 (0, 0.33)	2490.43	3529.27	1
ξ_1	Half-Cauchy(0,1)	0.8 (0, 3.64)	5527.61	4198.86	1
ξ_2	Half-Cauchy(0,1)	0.71 (0, 3.16)	5530.84	4354.07	1
ξ_3	Half-Cauchy(0,1)	0.7 (0, 3.17)	5619.71	4028.1	1
ξ_4	Half-Cauchy(0,1)	0.7 (0, 3.16)	5339.12	4298.68	1
ξ_5	Half-Cauchy(0,1)	0.87 (0, 4.74)	4017.01	3410.4	1
ξ_6	Half-Cauchy(0,1)	0.73 (0, 3.24)	5385.23	4137.06	1
ξ_7	Half-Cauchy(0,1)	1.91 (0, 11.22)	1908.35	1348.64	1
ξ_8	Half-Cauchy(0,1)	0.71 (0, 3.24)	3990.62	3145.32	1
ξ_9	Half-Cauchy(0,1)	0.76 (0, 3.46)	3943.2	3327.54	1
ξ_{10}	Half-Cauchy(0,1)	0.93 (0, 4.44)	3591.49	3176.66	1
ξ_{11}	Half-Cauchy(0,1)	0.78 (0, 3.69)	4937.19	3571.01	1
ξ_{12}	Half-Cauchy(0,1)	0.68 (0, 3)	4362.46	1313.24	1
ξ_{13}	Half-Cauchy(0,1)	0.74 (0, 3.43)	4566.12	2842.43	1
ξ_{14}	Half-Cauchy(0,1)	0.69 (0, 3.07)	5724.75	3701.21	1
ξ_{15}	Half-Cauchy(0,1)	0.8 (0, 3.84)	4790.29	4245.85	1
ξ_{16}	Half-Cauchy(0,1)	0.79 (0, 3.46)	3647.84	2712.66	1
ξ_{17}	Half-Cauchy(0,1)	0.77 (0, 3.43)	5954.65	4227.72	1
ξ_{18}	Half-Cauchy(0,1)	0.76 (0, 3.28)	5410.16	4099.88	1
ξ_{19}	Half-Cauchy(0,1)	0.76 (0, 3.82)	5667.42	3895.84	1
ξ_{20}	Half-Cauchy(0,1)	0.69 (0, 2.99)	5903.18	3498.75	1
logit(λ)	Normal(0,1)	0.31 (0.12, 0.49)	2332.48	1558.42	1
logit(ϵ)	Normal(0,1)	-5.75 (-5.98, -5.5)	3461.42	3211.9	1

Parameter estimates for full model fit to deep-sequence data from 1,970 RCCS participants living with viremic HIV with putative risk factors of harboring multiple infection and Bayesian shrinkage priors. ESS = effective sample size. HPD = highest posterior density.

References

1. Kijak GH, Sanders-Buell E, Chenine AL, Eller MA, Goonetilleke N, Thomas R, et al. Rare HIV-1 transmitted/founder lineages identified by deep viral sequencing contribute to rapid shifts in dominant quasiespecies during acute and early infection. *PLOS Pathogens*. 2017;13(7):e1006510. doi:10.1371/journal.ppat.1006510.
2. Redd AD, Quinn TC, Tobian AA. Frequency and implications of HIV superinfection. *The Lancet Infectious Diseases*. 2013;13(7):622–628. doi:10.1016/S1473-3099(13)70066-5.
3. Redd AD, Mullis CE, Serwadda D, Kong X, Martens C, Ricklefs SM, et al. The Rates of HIV Superinfection and Primary HIV Incidence in a General Population in Rakai, Uganda. *The Journal of Infectious Diseases*. 2012;206(2):267–274. doi:10.1093/infdis/jis325.
4. Wertheim JO, Oster AM, Murrell B, Saduvala N, Heneine W, Switzer WM, et al. Maintenance and reappearance of extremely divergent intra-host HIV-1 variants. *Virus Evolution*. 2018;4(2):vey030. doi:10.1093/ve/vey030.
5. Shriner D, Rodrigo AG, Nickle DC, Mullins JI. Pervasive Genomic Recombination of HIV-1 in Vivo. *Genetics*. 2004;167(4):1573–1583. doi:10.1534/genetics.103.023382.
6. Song H, Giorgi EE, Ganusov VV, Cai F, Athreya G, Yoon H, et al. Tracking HIV-1 recombination to resolve its contribution to HIV-1 evolution in natural infection. *Nature Communications*;9(1):1928. doi:10.1038/s41467-018-04217-5.
7. Streeck H, Li B, Poon AFY, Schneidewind A, Gladden AD, Power KA, et al. Immune-driven recombination and loss of control after HIV superinfection. *Journal of Experimental Medicine*. 2008;205(8):1789–1796. doi:10.1084/jem.20080281.
8. Ramirez BC, Simon-Loriere E, Galetto R, Negroni M. Implications of recombination for HIV diversity. *Virus Research*. 2008;134(1-2):64–73. doi:10.1016/j.virusres.2008.01.007.
9. Kim S, Kigozi G, Martin MA, Galiwango RM, Quinn TC, Redd AD, et al. Increasing intra- and inter-subtype HIV diversity despite declining HIV incidence in Uganda. *medRxiv*. 2024;doi:10.1101/2024.03.14.24303990.
10. Ritchie AJ, Cai F, Smith NM, Chen S, Song H, Brackenridge S, et al. Recombination-mediated escape from primary CD8+ T cells in acute HIV-1 infection. *Retrovirology*;11(1):69. doi:10.1186/s12977-014-0069-9.
11. Corey L, McElrath MJ. HIV vaccines: mosaic approach to virus diversity. *Nature Medicine*. 2010;16(3):268–270. doi:10.1038/nm0310-268.
12. Kiwanuka N, Laeyendecker O, Quinn TC, Wawer MJ, Shepherd J, Robb M, et al. HIV-1 subtypes and differences in heterosexual HIV transmission among HIV-discordant couples in Rakai, Uganda. *AIDS*. 2009;23(18):2479–2484. doi:10.1097/QAD.0b013e328330cc08.
13. Gottlieb GS, Nickle DC, Jensen MA, Wong KG, Grobler J, Li F, et al. Dual HIV-1 infection associated with rapid disease progression. *The Lancet*. 2004;363(9409):619–622. doi:10.1016/S0140-6736(04)15596-7.
14. Smith DM. Incidence of HIV Superinfection Following Primary Infection. *JAMA: The Journal of the American Medical Association*. 2004;292(10):1177–1178. doi:10.1001/jama.292.10.1177.
15. Ronen K, Richardson BA, Graham SM, Jaoko W, Mandaliya K, McClelland RS, et al. HIV-1 superinfection is associated with an accelerated viral load increase but has a limited impact on disease progression. *AIDS*. 2014;28(15):2281–2286. doi:10.1097/QAD.0000000000000422.

16. Janes H, Herbeck JT, Tovanabutra S, Thomas R, Frahm N, Duerr A, et al. HIV-1 infections with multiple founders are associated with higher viral loads than infections with single founders. *Nature Medicine*. 2015;21(10):1139–1141. doi:10.1038/nm.3932.
17. Quinn TC, Wawer MJ, Sewankambo N, Serwadda D, Li C, Wabwire-Mangen F, et al. Viral Load and Heterosexual Transmission of Human Immunodeficiency Virus Type 1. *New England Journal of Medicine*. 2000;342(13):921–929. doi:10.1056/NEJM200003303421303.
18. Fraser C, Hollingsworth TD, Chapman R, de Wolf F, Hanage WP. Variation in HIV-1 set-point viral load: Epidemiological analysis and an evolutionary hypothesis. *Proceedings of the National Academy of Sciences*. 2007;104(44):17441–17446. doi:10.1073/pnas.0708559104.
19. Yuan D, Zhao F, Liu S, Liu Y, Yan H, Liu L, et al. Dual Infection of Different Clusters of HIV in People Living with HIV Worldwide: A Meta-Analysis Based on Next-Generation Sequencing Studies. *AIDS Patient Care and STDs*. 2024; p. apc.2024.0100. doi:10.1089/apc.2024.0100.
20. Cornelissen M, Jurriaans S, Kozaczynska K, Prins JM, Hamidjaja RA, Zorgdrager F, et al. Routine HIV-1 genotyping as a tool to identify dual infections. *AIDS*. 2007;21(7):807–811. doi:10.1097/QAD.0b013e3280f3c08a.
21. van der Kuyl AC, Zorgdrager F, Jurriaans S, Back NKT, Prins JM, Brinkman K, et al. Incidence of Human Immunodeficiency Virus Type 1 Dual Infections in Amsterdam, The Netherlands, during 2003–2007. *Clinical Infectious Diseases*. 2009;48(7):973–978. doi:10.1086/597356.
22. Chaudron SE, Leemann C, Kusejko K, Nguyen H, Tschumi N, Marzel A, et al. A Systematic Molecular Epidemiology Screen Reveals Numerous Human Immunodeficiency Virus (HIV) Type 1 Superinfections in the Swiss HIV Cohort Study. *The Journal of Infectious Diseases*. 2022;226(7):1256–1266. doi:10.1093/infdis/jiac166.
23. Rachinger A, van de Ven TD, Burger JA, Schuitemaker H, van 't Wout AB. Evaluation of pre-screening methods for the identification of HIV-1 superinfection. *Journal of Virological Methods*. 2010;165(2):311–317. doi:https://doi.org/10.1016/j.jviromet.2010.02.016.
24. Pacold M, Smith D, Little S, Cheng PM, Jordan P, Ignacio C, et al. Comparison of Methods to Detect HIV Dual Infection. *AIDS Research and Human Retroviruses*. 2010;26(12):1291–1298. doi:10.1089/aid.2010.0042.
25. Keele BF, Giorgi EE, Salazar-Gonzalez JF, Decker JM, Pham KT, Salazar MG, et al. Identification and characterization of transmitted and early founder virus envelopes in primary HIV-1 infection. *Proceedings of the National Academy of Sciences*. 2008;105(21):7552–7557. doi:10.1073/pnas.0802203105.
26. Abrahams MR, Anderson JA, Giorgi EE, Seoighe C, Mlisana K, Ping LH, et al. Quantitating the Multiplicity of Infection with Human Immunodeficiency Virus Type 1 Subtype C Reveals a Non-Poisson Distribution of Transmitted Variants. *Journal of Virology*. 2009;83(8):3556–3567. doi:10.1128/JVI.02132-08.
27. Li H, Bar KJ, Wang S, Decker JM, Chen Y, Sun C, et al. High Multiplicity Infection by HIV-1 in Men Who Have Sex with Men. *PLoS Pathogens*. 2010;6(5):e1000890. doi:10.1371/journal.ppat.1000890.
28. Dwyer-Lindgren L, Cork MA, Sligar A, Steuben KM, Wilson KF, Provost NR, et al. Mapping HIV prevalence in sub-Saharan Africa between 2000 and 2017. *Nature*. 2019;570(7760):189–193. doi:10.1038/s41586-019-1200-9.
29. Redd AD, Collinson-Streng A, Martens C, Ricklefs S, Mullis CE, Manucci J, et al. Identification of HIV Superinfection in Seroconcordant Couples in Rakai, Uganda, by Use of Next-Generation Deep Sequencing. *Journal of Clinical Microbiology*. 2011;49(8):2859–2867. doi:10.1128/jcm.00804-11.
30. Redd AD, Ssemwanga D, Vandepitte J, Wendel SK, Ndembu N, Bukonya J, et al. Rates of HIV-1 superinfection and primary HIV-1 infection are similar in female sex workers in Uganda. *AIDS*. 2014;28(14):2147–2152. doi:10.1097/QAD.0000000000000365.

31. Ronen K, McCoy CO, Matsen FA, Boyd DF, Emery S, Odem-Davis K, et al. HIV-1 Superinfection Occurs Less Frequently Than Initial Infection in a Cohort of High-Risk Kenyan Women. *PLoS Pathogens*. 2013;9(8):e1003593. doi:10.1371/journal.ppat.1003593. 676 677 678
32. Piantadosi A, Ngayo MO, Chohan B, Overbaugh J. Examination of a Second Region of the HIV Type 1 Genome Reveals Additional Cases of Superinfection. *AIDS Research and Human Retroviruses*. 2008;24(9):1221–1224. doi:10.1089/aid.2008.0100. 679 680 681
33. Bonsall D, Golubchik T, de Cesare M, Limbada M, Kosloff B, MacIntyre-Cockett G, et al. A Comprehensive Genomics Solution for HIV Surveillance and Clinical Monitoring in Low-Income Settings. *Journal of Clinical Microbiology*. 2020;58(10):e00382–20. doi:10.1128/JCM.00382-20. 682 683 684
34. Gall A, Ferns B, Morris C, Watson S, Cotten M, Robinson M, et al. Universal Amplification, Next-Generation Sequencing, and Assembly of HIV-1 Genomes. *Journal of Clinical Microbiology*. 2012;50(12):3838–3844. doi:10.1128/JCM.01516-12. 685 686 687
35. Grabowski MK, Serwadda DM, Gray RH, Nakigozi G, Kigozi G, Kagaayi J, et al. HIV Prevention Efforts and Incidence of HIV in Uganda. *New England Journal of Medicine*. 2017;377(22):2154–2166. doi:10.1056/NEJMoa1702150. 688 689 690
36. Chang LW, Grabowski MK, Ssekubugu R, Nalugoda F, Kigozi G, Nantume B, et al. Heterogeneity of the HIV epidemic in agrarian, trading, and fishing communities in Rakai, Uganda: an observational epidemiological study. *The Lancet HIV*. 2016;3(8):e388–e396. doi:10.1016/S2352-3018(16)30034-0. 691 692 693
37. Wymant C, Hall M, Ratmann O, Bonsall D, Golubchik T, Cesare MD, et al. PHYLOSCANNER: Inferring Transmission from Within- and Between-Host Pathogen Genetic Diversity. *Molecular Biology And Evolution*. 2017;35(3):719–733. doi:10.1093/molbev/msx304. 694 695 696
38. Monod M, Brizzi A, Galiwango RM, Ssekubugu R, Chen Y, Xi X, et al. Longitudinal population-level HIV epidemiologic and genomic surveillance highlights growing gender disparity of HIV transmission in Uganda. *Nature Microbiology*. 2023;9(1):35–54. doi:10.1038/s41564-023-01530-8. 697 698 699
39. Dambach P, Mahenge B, Mashasi I, Muya A, Barnhart DA, Bärnighausen TW, et al. Socio-demographic characteristics and risk factors for HIV transmission in female bar workers in sub-Saharan Africa: a systematic literature review. *BMC Public Health*. 2020;20(1):697. doi:10.1186/s12889-020-08838-8. 700 701 702
40. Popoola VO, Kagaayi J, Ssekasanvu J, Ssekubugu R, Kigozi G, Ndyababo A, et al. HIV epidemiologic trends among occupational groups in Rakai, Uganda: A population-based longitudinal study, 1999–2016. *PLOS Global Public Health*. 2024;4(2):1–18. doi:10.1371/journal.pgph.0002891. 703 704 705
41. Global Aids response progress report: Uganda January 2010–December 2012;. 706
42. Kagulire SC, Opendi P, Stamper PD, Nakavuma JL, Mills LA, Makumbi F, et al. Field evaluation of five rapid diagnostic tests for screening of HIV-1 infections in rural Rakai, Uganda. *International Journal of STD & AIDS*. 2011;22(6):308–309. doi:10.1258/ijsa.2009.009352. 707 708 709
43. Pillay D, Herbeck J, Cohen MS, Oliveira TD, Fraser C, Ratmann O, et al. PANGAEA-HIV: phylogenetics for generalised epidemics in Africa. *The Lancet Infectious Diseases*. 2015;15(3):259–261. doi:10.1016/S1473-3099(15)70036-8. 710 711 712
44. Abeler-Dörner L, Grabowski MK, Rambaut A, Pillay D, Fraser C. PANGAEA-HIV 2: Phylogenetics And Networks for Generalised Epidemics in Africa. *Current Opinion in HIV and AIDS*. 2019;14(3):173–180. doi:10.1097/COH.0000000000000542. 713 714 715
45. Wood DE, Salzberg SL. Kraken: Ultrafast metagenomic sequence classification using exact alignments. *Genome Biology*. 2014;15(3). doi:10.1186/gb-2014-15-3-r46. 716 717
46. Bolger AM, Lohse M, Usadel B. Trimmomatic: A flexible trimmer for Illumina sequence data. *Bioinformatics*. 2014;30(15):2114–2120. doi:10.1093/bioinformatics/btu170. 718 719

47. Bankevich A, Nurk S, Antipov D, Gurevich AA, Dvorkin M, Kulikov AS, et al. SPAdes: A New
Genome Assembly Algorithm and Its Applications to Single-Cell Sequencing. *Journal of Computational
Biology*. 2012;19(5):455–477. doi:10.1089/cmb.2012.0021. 720 721 722
48. Nurk S, Meleshko D, Korobeynikov A, Pevzner PA. metaSPAdes: a new versatile metagenomic
assembler. *Genome Research*. 2024;27(5):824–834. doi:10.1101/gr.213959.116. 723 724
49. Wymant C, Blanquart F, Golubchik T, Gall A, Bakker M, Bezemer D, et al. Easy and accurate
reconstruction of whole HIV genomes from short-read sequence data with shiver. *Virus Evolution*.
2018;4(1). doi:10.1093/ve/vey007. 725 726 727
50. Xi X. Bayesian methods for source attribution using HIV deep sequence data.
2021;doi:10.25560/101957. 728 729
51. Lynch RM, Shen T, Gnanakaran S, Derdeyn CA. Appreciating HIV Type 1 Diversity: Subtype Differ-
ences in Env. *AIDS Research and Human Retroviruses*. 2009;25(3):237–248. doi:10.1089/aid.2008.0219. 730 731
52. Katoh K, Misawa K, Kuma Ki, Miyata T. MAFFT: a novel method for rapid multiple se-
quence alignment based on fast Fourier transform. *Nucleic acids research*. 2002;30(14):3059–3066.
doi:10.1093/nar/gkf436. 732 733 734
53. Nguyen LT, Schmidt HA, Von Haeseler A, Minh BQ. IQ-TREE: A fast and effective stochas-
tic algorithm for estimating maximum-likelihood phylogenies. *Molecular Biology and Evolution*.
2015;32(1):268–274. doi:10.1093/molbev/msu300. 735 736 737
54. Minh BQ, Schmidt HA, Chernomor O, Schrempf D, Woodhams MD, Von Haeseler A, et al. IQ-TREE
2: New Models and Efficient Methods for Phylogenetic Inference in the Genomic Era. *Molecular
Biology and Evolution*. 2020;37(5):1530–1534. doi:10.1093/molbev/msaa015. 738 739 740
55. Ratmann O, Grabowski MK, Hall M, Golubchik T, Wymant C, Abeler-Dörner L, et al. Inferring
HIV-1 transmission networks and sources of epidemic spread in Africa with deep-sequence phylogenetic
analysis. *Nature Communications*. 2019;10(1):1411. doi:10.1038/s41467-019-09139-4. 741 742 743
56. Sankoff D. Minimal Mutation Trees of Sequences. *SIAM Journal on Applied Mathematics*.
1975;28(1):35–42. doi:10.1137/0128004. 744 745
57. Stan Modeling Language Users Guide and Reference Manual, Version 2.35;. Available from: <https://mc-stan.org>. 746 747
58. Carvalho CM, Polson NG, Scott JG. Handling Sparsity via the Horseshoe. In: van Dyk D, Welling M,
editors. *Proceedings of the Twelfth International Conference on Artificial Intelligence and Statistics*.
vol. 5 of *Proceedings of Machine Learning Research*. Hilton Clearwater Beach Resort, Clearwater
Beach, Florida USA: PMLR; 2009. p. 73–80. Available from: [https://proceedings.mlr.press/v5/
carvalho09a.html](https://proceedings.mlr.press/v5/carvalho09a.html). 748 749 750 751 752
59. Piironen J, Vehtari A. Sparsity information and regularization in the horseshoe and other shrinkage
priors. *Electronic Journal of Statistics*. 2017;11(2):5018 – 5051. doi:10.1214/17-EJS1337SI. 753 754
60. Betancourt MJ, Girolami M. Hamiltonian Monte Carlo for Hierarchical Models; 2013. Available from:
<https://arxiv.org/abs/1312.0906>. 755 756
61. Hoffman MD, Gelman A. The No-U-Turn Sampler: Adaptively Setting Path Lengths in Hamiltonian
Monte Carlo. *Journal of Machine Learning Research*. 2014;15(47):1593–1623. 757 758
62. Gabry J, Češnovar R, Johnson A. cmdstanr: R Interface to 'CmdStan'; 2023. 759
63. Vehtari A, Gelman A, Simpson D, Carpenter B, Bürkner PC. Rank-Normalization, Folding, and
Localization: An Improved \hat{R} for Assessing Convergence of MCMC (with Discussion). *Bayesian
Analysis*. 2021;16(2). doi:10.1214/20-BA1221. 760 761 762

64. R Core Team. R: A Language and Environment for Statistical Computing; 2023. Available from: <https://www.R-project.org/>. 763 764
65. Wickham H, Averick M, Bryan J, Chang W, McGowan LD, François R, et al. Welcome to the tidyverse. *Journal of Open Source Software*. 2019;4(43):1686. doi:10.21105/joss.01686. 765 766
66. Wickham H, François R, Henry L, Müller K, Vaughan D. dplyr: A Grammar of Data Manipulation; 2023. Available from: <https://CRAN.R-project.org/package=dplyr>. 767 768
67. Müller K, Wickham H. tibble: Simple Data Frames; 2023. Available from: <https://CRAN.R-project.org/package=tibble>. 769 770
68. Wickham H, Vaughan D, Girlich M. tidyr: Tidy Messy Data; 2024. Available from: <https://CRAN.R-project.org/package=tidyr>. 771 772
69. Wickham H, Miller E, Smith D. haven: Import and Export 'SPSS', 'Stata' and 'SAS' Files; 2023. Available from: <https://haven.tidyverse.org>. 773 774
70. Wickham H. ggplot2: Elegant Graphics for Data Analysis. Springer-Verlag New York; 2016. Available from: <https://ggplot2.tidyverse.org>. 775 776
71. Gabry J, Mahr T. bayesplot: Plotting for Bayesian Models; 2024. Available from: <https://mc-stan.org/bayesplot/>. 777 778
72. Gabry J, Simpson D, Vehtari A, Betancourt M, Gelman A. Visualization in Bayesian workflow. *J R Stat Soc A*. 2019;182:389–402. doi:10.1111/rssa.12378. 779 780
73. Wilke CO. cowplot: Streamlined Plot Theme and Plot Annotations for 'ggplot2'; 2024. Available from: <https://wilkelab.org/cowplot/>. 781 782
74. Pedersen TL. patchwork: The Composer of Plots; 2024. Available from: <https://patchwork.data-imaginist.com>. 783 784
75. Paradis E, Schliep K. ape 5.0: an environment for modern phylogenetics and evolutionary analyses in R. *Bioinformatics*. 2019;35:526–528. doi:10.1093/bioinformatics/bty633. 785 786
76. Yu G. Data Integration, Manipulation and Visualization of Phylogenetic Treess. 1st ed. Chapman and Hall/CRC; 2022. Available from: <https://www.amazon.com/Integration-Manipulation-Visualization-Phylogenetic-Computational-ebook/dp/B0B5NLZR1Z/>. 787 788 789 790
77. Xu S, Li L, Luo X, Chen M, Tang W, Zhan L, et al. Ggtree: A serialized data object for visualization of a phylogenetic tree and annotation data. *iMeta*. 2022;1(4):e56. doi:10.1002/imt2.56. 791 792
78. Yu G. Using ggtree to Visualize Data on Tree-Like Structures. *Current Protocols in Bioinformatics*. 2020;69(1):e96. doi:10.1002/cpbi.96. 793 794
79. Yu G, Lam TTY, Zhu H, Guan Y. Two methods for mapping and visualizing associated data on phylogeny using ggtree. *Molecular Biology and Evolution*. 2018;35:3041–3043. doi:10.1093/molbev/msy194. 795 796 797
80. Yu G, Smith D, Zhu H, Guan Y, Lam TTY. ggtree: an R package for visualization and annotation of phylogenetic trees with their covariates and other associated data. *Methods in Ecology and Evolution*. 2017;8:28–36. doi:10.1111/2041-210X.12628. 798 799 800
81. Revell LJ. phytools 2.0: an updated R ecosystem for phylogenetic comparative methods (and other things). *PeerJ*. 2024;12:e16505. doi:10.7717/peerj.16505. 801 802
82. Meredith M, Kruschke J. HDInterval: Highest (Posterior) Density Intervals; 2022. Available from: <https://CRAN.R-project.org/package=HDInterval>. 803 804

83. Bürkner PC, Gabry J, Kay M, Vehtari A. posterior: Tools for Working with Posterior Distributions; 2023. Available from: <https://mc-stan.org/posterior/>. 805 806
84. Delignette-Muller ML, Dutang C. fitdistrplus: An R Package for Fitting Distributions. *Journal of Statistical Software*. 2015;64(4):1–34. doi:10.18637/jss.v064.i04. 807 808
85. PANGAEA-HIV/PANGAEA-Sequences: Latest Version Release; 2024. Available from: <https://doi.org/10.5281/zenodo.10793873>. 809 810
86. Ratmann O, Wymant C, Colijn C, Danaviah S, Essex M, Frost S, et al. HIV-1 Full-Genome Phylogenetics of Generalized Epidemics in Sub-Saharan Africa: Impact of Missing Nucleotide Characters in Next-Generation Sequences. *AIDS Research and Human Retroviruses*. 2017;33(11):1083–1098. doi:10.1089/aid.2017.0061. 811 812 813 814
87. Désiré N, Cerutti L, Le Hingrat Q, Perrier M, Emler S, Calvez V, et al. Characterization update of HIV-1 M subtypes diversity and proposal for subtypes A and D sub-subtypes reclassification. *Retrovirology*. 2018;15(1):80. doi:10.1186/s12977-018-0461-y. 815 816 817
88. Patiño-Galindo JÁ, González-Candelas F. The substitution rate of HIV-1 subtypes: a genomic approach. *Virus Evolution*. 2017;3(2). doi:10.1093/ve/vex029. 818 819
89. Brizzi A, Kagaayi J, Ssekubugu R, Abeler-Dörner L, Blenkinsop A, Bonsall D, et al. Age and gender profiles of HIV infection burden and viraemia: novel metrics for HIV epidemic control in African populations with high antiretroviral therapy coverage. *medRxiv*. 2024;doi:10.1101/2024.04.21.24306145. 820 821 822
90. Todd J, Cremin I, McGrath N, Bwanika JB, Wringe A, Marston M, et al. Reported number of sexual partners: comparison of data from four African longitudinal studies. *Sexually Transmitted Infections*. 2009;85:i72–i80. doi:10.1136/sti.2008.033985. 823 824 825
91. Pacold ME, Pond SLK, Wagner GA, Delport W, Bourque DL, Richman DD, et al. Clinical, virologic, and immunologic correlates of HIV-1 intraclade B dual infection among men who have sex with men. *AIDS*. 2012;26(2):157–165. doi:10.1097/QAD.0b013e32834dcd26. 826 827 828
92. Wagner GA, Pacold ME, Vigil E, Caballero G, Morris SR, Kosakovsky Pond SL, et al. Using Ultradeep Pyrosequencing to Study HIV-1 Coreceptor Usage in Primary and Dual Infection. *The Journal of Infectious Diseases*. 2013;208(2):271–274. doi:10.1093/infdis/jit168. 829 830 831
93. Wagner GA, Pacold ME, Kosakovsky Pond SL, Caballero G, Chaillon A, Rudolph AE, et al. Incidence and Prevalence of Intrasubtype HIV-1 Dual Infection in At-Risk Men in the United States. *The Journal of Infectious Diseases*. 2014;209(7):1032–1038. doi:10.1093/infdis/jit633. 832 833 834
94. Wagner GA, Chaillon A, Liu S, Franklin DR, Caballero G, Kosakovsky Pond SL, et al. HIV-associated neurocognitive disorder is associated with HIV-1 dual infection. *AIDS*. 2016;30(17):2591–2597. doi:10.1097/QAD.0000000000001237. 835 836 837
95. Vesa J, Chaillon A, Wagner GA, Anderson CM, Richman DD, Smith DM, et al. Increased HIV-1 superinfection risk in carriers of specific human leukocyte antigen alleles. *AIDS*. 2017;31(8):1149–1158. doi:10.1097/QAD.0000000000001445. 838 839 840
96. Patel P, Borkowf CB, Brooks JT, Lasry A, Lansky A, Mermin J. Estimating per-act HIV transmission risk: a systematic review. *AIDS*. 2014;28(10):1509–1519. doi:10.1097/QAD.0000000000000298. 841 842
97. Kate Grabowski M, Lessler J, Bazaale J, Nabukalu D, Nankinga J, Nantume B, et al. Migration, hotspots, and dispersal of HIV infection in Rakai, Uganda. *Nature Communications*. 2020;11(1):976. doi:10.1038/s41467-020-14636-y. 843 844 845
98. Ratmann O, Kagaayi J, Hall M, Golubchick T, Kigozi G, Xi X, et al. Quantifying HIV transmission flow between high-prevalence hotspots and surrounding communities: a population-based study in Rakai, Uganda. *The Lancet HIV*. 2020;7(3):e173–e183. doi:10.1016/S2352-3018(19)30378-9. 846 847 848

99. Kagaayi J, Chang LW, Ssempijja V, Grabowski MK, Ssekubugu R, Nakigozi G, et al. Impact of combination HIV interventions on HIV incidence in hyperendemic fishing communities in Uganda: a prospective cohort study. *The Lancet HIV*;6(10):e680–e687. doi:10.1016/S2352-3018(19)30190-0. 849 850 851
100. Martin MA, Reynolds SJ, Ssuuna C, Foley BT, Nalugoda F, Quinn TC, et al. Population dynamics of HIV drug resistance among pre-treatment and treatment-experienced persons with HIV during treatment scale-up in Uganda: a population-based longitudinal study. *medRxiv*. 2023;doi:10.1101/2023.10.14.23297021. 852 853 854 855
101. Rambaut A, Posada D, Crandall KA, Holmes EC. The causes and consequences of HIV evolution. *Nature Reviews Genetics*. 2004;5(1):52–61. doi:10.1038/nrg1246. 856 857
102. Cunningham EB, Applegate TL, Lloyd AR, Dore GJ, Grebely J. Mixed HCV infection and reinfection in people who inject drugs—impact on therapy. *Nature Reviews Gastroenterology & Hepatology*. 2015;12(4):218–230. doi:10.1038/nrgastro.2015.36. 858 859 860
103. Van De Laar TJW, Molenkamp R, Van Den Berg C, Schinkel J, Beld MGHM, Prins M, et al. Frequent HCV reinfection and superinfection in a cohort of injecting drug users in Amsterdam. *Journal of Hepatology*. 2009;51(4):667–674. doi:10.1016/j.jhep.2009.05.027. 861 862 863
104. Eliseev A, Gibson KM, Avdeyev P, Novik D, Bendall ML, Pérez-Losada M, et al. Evaluation of haplotype callers for next-generation sequencing of viruses. *Infection, Genetics and Evolution*. 2020;82:104277. doi:10.1016/j.meegid.2020.104277. 864 865 866
105. Cohen T, Van Helden PD, Wilson D, Colijn C, McLaughlin MM, Abubakar I, et al. Mixed-Strain *Mycobacterium tuberculosis* Infections and the Implications for Tuberculosis Treatment and Control. *Clinical Microbiology Reviews*. 2012;25(4):708–719. doi:10.1128/CMR.00021-12. 867 868 869
106. Sobkowiak B, Glynn JR, Houben RMGJ, Mallard K, Phelan JE, Guerra-Assunção JA, et al. Identifying mixed *Mycobacterium tuberculosis* infections from whole genome sequence data. *BMC Genomics*. 2018;19(1):613. doi:10.1186/s12864-018-4988-z. 870 871 872
107. Gabbassov E, Moreno-Molina M, Comas I, Libbrecht M, Chindelevitch L. SplitStrains, a tool to identify and separate mixed *Mycobacterium tuberculosis* infections from WGS data. *Microbial Genomics*. 2021;7(6). doi:10.1099/mgen.0.000607. 873 874 875
108. Sobkowiak B, Cudahy P, Chitwood MH, Clark TG, Colijn C, Grandjean L, et al. A new method for detecting mixed *Mycobacterium tuberculosis* infection and reconstructing constituent strains provides insights into transmission. *bioRxiv*. 2024;doi:10.1101/2024.04.26.591283. 876 877 878
109. Anyansi C, Keo A, Walker BJ, Straub TJ, Manson AL, Earl AM, et al. QuantTB – a method to classify mixed *Mycobacterium tuberculosis* infections within whole genome sequencing data. *BMC Genomics*. 2020;21(1):80. doi:10.1186/s12864-020-6486-3. 879 880 881
110. Dezordi FZ, Resende PC, Naveca FG, Do Nascimento VA, De Souza VC, Dias Paixão AC, et al. Unusual SARS-CoV-2 intrahost diversity reveals lineage superinfection. *Microbial Genomics*. 2022;8(3). doi:10.1099/mgen.0.000751. 882 883 884
111. Wertheim JO, Wang JC, Leelawong M, Martin DP, Havens JL, Chowdhury MA, et al. Detection of SARS-CoV-2 intra-host recombination during superinfection with Alpha and Epsilon variants in New York City. *Nature Communications*. 2022;13(1):3645. doi:10.1038/s41467-022-31247-x. 885 886 887